NUTRIENT REMOVAL FROM TREATED EFFLUENT OF A 3 MLD SEWAGE TREATMENT PLANT USING BIOCHAR ADSORBENT IN FIXED BED COLUMN

A Dissertation

submitted in partial fulfillment of the requirement

for the award of degree of

Masters in Technology

in

Environmental Science and Technology

Submitted by

Nehaun

Roll No.: 602101007

Under the Guidance of

Dr. Gaurav Goel

Assistant Professor

Absar Ahmad Kazmi

Professor

Civil Eng. Department, IITR

THAPAR INSTITUTE
OF ENGINEERING & TECHNOLOGY
(Deemed to be University)

SCHOOL OF ENERGY AND ENVIRONMENT

THAPAR INSTITUTE OF ENGINEERING & TECHNOLOGY, PATIALA

July 2023

सिविल इंजीनियरिंग विभाग
भारतीय प्रौद्योगिकी संस्थान, रुड़की - 247 667 (उत्तराखण्ड) भारत
DEPARTMENT OF CIVIL ENGINEERING
INDIAN INSTITUTE OF TECHNOLOGY, ROORKEE - 247 667 (U.K.) INDIA

Dr. A. A. Kazmi
D. Engg. (Tokyo Univ.), M. Engg. (A.I.T. Bangkok)
B. Engg. (Hons.) (AMU)
Professor

Fax : +91-1332-275568
Phone: +91-1332-285725 (O), 284257 (Lab)
+91-1332-285226 (R)
Mob. : +91-9837262698
e-mail : absar.kazmi@ce.iitr.ac.in
absarakazmi@yahoo.com

Dated: 10/07/2023

TO WHOMSOEVER IT MAY CONCERN

This is to certify that Ms. Nehaun from the School of Energy and Environment, Thapar Institute of Engineering and Technology Patiala has successfully completed her Dissertation under my Co Supervision on the project "**Nutrient removal from treated effluent of a 3 MLD sewage treatment plant using biochar adsorbent in fixed bed column**" in the Department of Civil Engineering, Indian Institute of Technology (IIT) Roorkee, from 15.06.22 to 14.06.23.

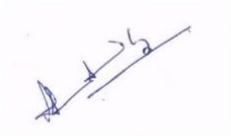

A. A. Kazmi

DECLARATION CUM CERTIFICATE

I hereby declare that the project work entitled "**Nutrient removal from treated effluent of a 3 MLD sewage treatment plant using biochar adsorbent in fixed bed column**" is an authentic record of my work carried out at the **Indian Institute of Technology Roorkee** as requirement of a one-year project internship for the award of the degree of M.Tech., Environmental Science and Technology, TIET, Patiala, under the guidance of Prof. Absar Ahmad Kazmi and Dr. Gaurav Goel, during June 2022 to June 2023

Nehaun

Nehaun

602101007

Date: 07-07-2023

Certified that the above statement made by the student is correct to the best of our knowledge and belief.

Gaurav Goel

Dr. Gaurav Goel

Assistant Professor

Absar Ahmad Kazmi

Professor

ACKNOWLEDGEMENT

First and foremost, I would like to express my sincere thankfulness to Allah for protecting and providing me with countless blessings, knowledge, opportunities, and the willpower to get through challenging moments.

It is a great pleasure to express my heartfelt gratitude to various people who have encouraged and supported me throughout. I am deeply grateful to both of my research guides, **Dr. Gaurav Goel** and **Prof A.A. Kazmi** for their invaluable guidance and support. I deeply acknowledge their motivation, patience, and immense knowledge which is a constant help for me in my research.

I am thankful to the Civil Department of the Indian Institute of Technology, Roorkee for granting permission to conduct my research in their department.

I would like to thank **Dr. Muntazir Ali** who keeps providing me with his timely and invaluable expert assistance.

I want to extend my sincere gratitude to **Dr. Shilpi Verma**, the internship coordinator, for her essential help and direction., for her invaluable support and guidance.

I would also like to express my deepest gratitude to all the faculty members in the **School of Energy and Environment**, for providing me with an opportunity to undergo this project.

I would like to express high regard to my parents for their continuous encouragement and prayers, which helps me easily handle even difficult situations. I am infinitely indebted to them for raising me to be the person I am today.

July 2023 Nehaun

TIET, Patiala

ABSTRACT

Our study aims for the green synthesis of an effective biochar adsorbent from Agro-waste to remove additional nutrients such as nitrogen and phosphorus from the treated effluent of 3MLD SBR STP at IIT Roorkee campus. The biochar adsorbent was successfully synthesized via single-step from agricultural waste i.e., sugarcane bagasse by pyrolysis process in presence of nitrogen gas at 550℃ for 30 min, 45 min, 1 hr., and 1 hr. 15 min. The material was further characterized by Raman spectroscopy, Fourier transform infrared spectroscopy (FTIR), Scanning electron microscopy (SEM) coupled with Energy dispersive X-ray analysis (EDX), and X-ray powder diffraction (XRD). For the optimization of removal of additional nutrients, four experimental columns made of borosilicate glass with an internal diameter of 30 mm and a length of 250 mm. All 04 columns were packed with the different adsorbent materials (35 mm) varying in preparation time viz. 30 min., 45 min., 1 hr., and 1 hr. 15 min. respectively between the supporting layers of glass wool (10 mm) each (for improving the flow distribution and prevention of the loss of adsorbent), and gravel (105mm and 90 mm). The Peristaltic pump was used to draw water from the inlet water can to the column. The up-flow mode was used to prevent channeling and assure consistent streaming. Columns of diameter 3.0cm and length 25.0cm were fabricated with four different materials (varying in their preparation time). The effect of initial adsorbate concentration, and the flow rate of adsorbate in the column were studied for the optimization of the adsorption column setup. Initially, there was an increase in the pH of the adsorbate by 3% for almost one week indicating the release of alkali ions from the adsorbent. The maximum bed capacity was obtained at the lowest flowrate and a highest initial concentration. The experimental data were fitted with different models such as the Thomas, Yoon-Nelson and, Adam-Bohart models. Both Thomas and Yoon-Nelson model were

found to show a good agreement with the experimental data as compared to Adam-Bohart model.

TABLE OF CONTENTS

LIST OF ABBREVIATIONS

ABBREVIATION	MEANING
STP	Sewage Treatment Plant
COD	Chemical Oxygen Demand
SBR	Sequencing Batch Reactor
NH_4-N	Ammonium ion
PO_4-P	Phosphate ion
NO_3-N	Nitrate Nitrogen
RGO	Reduced Graphene Oxide
ICMBBR	Intermittent cycle moving bed biofilm reactor
TN	Total Nitrogen
TP	Total Phosphorous
TKN	Total Kjeldahl Nitrogen
BES	Bioelectrochemical Systems
XRD	X-ray powder diffraction
FTIR	Fourier transform infrared spectroscopy
FE-SEM	Field Emission Scanning Electron Microscopy
MLD	Million Liters per Day

BOD	Biochemical oxygen demand
TSS	Total Suspended Solids
SEM	Scanning electron microscopy

NOTATIONS

SYMBOL	DESCRIPTIONS	UNITS
C_i	Influent concentration	mg L^{-1}
C_f	Effluent concentration	mg L^{-1}
k_{TH}	Thomas rate constant	ml min^{-1} mg^{-1}
q_0	Maximum solid-phase concentration of solute or adsorption capacity	mg g^{-1}
w	Mass of the adsorbent in column	g
Q	Flow rate	ml min^{-1}
t	Total flow time	min
k_{AB}	Kinetic constant	ml min^{-1} mg^{-1}
N_0	Sorption capacity	mg L^{-1}
z	Bed-depth	cm
u	Linear velocity	Mm h^{-1}
k_{YN}	Rate constant	ml min^{-1} mg^{-1}
τ	Time required for 50% sorbate breakthrough	min

LIST OF FIGURES

LIST OF TABLES

CHAPTER 1

INTRODUCTION

1.1 Objective

One of the most common reasons for poor water quality is nutrient pollution. Aquatic ecosystems are being harmed by nutrient pollution, which has detrimental effects on the economy, a decline in biodiversity, and concern for human health. Nutrient pollution comes from a variety of sources, but contributions from human waste, such as wastewater and fecal sludge containing compounds of carbon, nitrogen, and phosphorus, are especially alarming (3). For this reason, phosphorus, nitrogen, carbon, and other micronutrients present in wastewater in wastewater treatment units should meet standard effluent limits for nutrients.

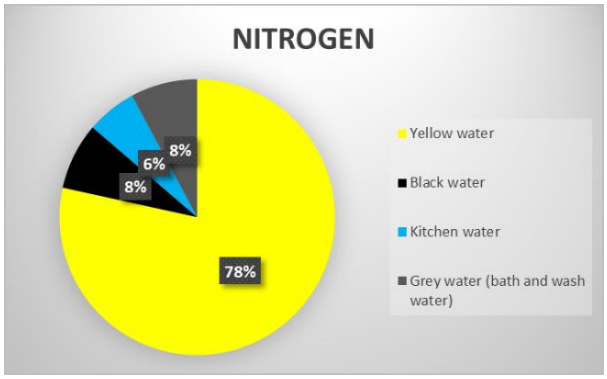

Figure 1.1: Various sources of Nitrogen constituent loading in Residential wastewater(51)

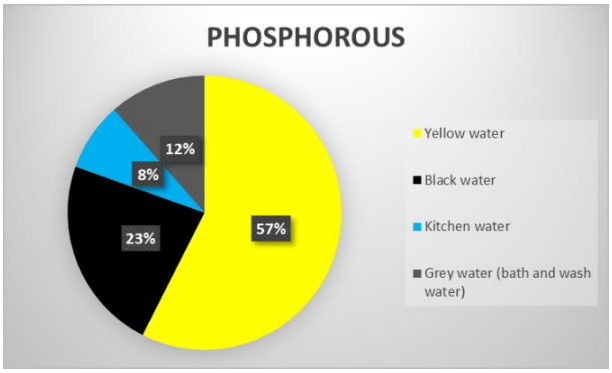

Figure 1.2: Various sources of Phosphorous constituent loading in Residential wastewater(51)

In receiving waterbodies, nitrogen and phosphorus concentrations are rising, leading to Eutrophication increasing aquatic and marine ecosystem damage by steering algal blooms, low DO concentrations, and dead zones or hypoxia. Additionally, the development of algae brought on by nutrient pollution produces carbon dioxide, which aids in the acidification of estuaries and coasts.

The nitrogenous compounds, also known as Total Nitrogen, include oxidized nitrogen molecules like nitrate and nitrite, as well as organic nitrogen and inorganic total ammonia nitrogen, which are collectively represented by the Total Kjeldahl Nitrogen. Ammonia and ammonium nitrogen make up the inorganic total ammonia nitrogen (1). In adults, an excess of nitrate anions is what causes diseases like stomach cancer, shortness of breath, a quick heartbeat, frequent urination, and physical collapse.

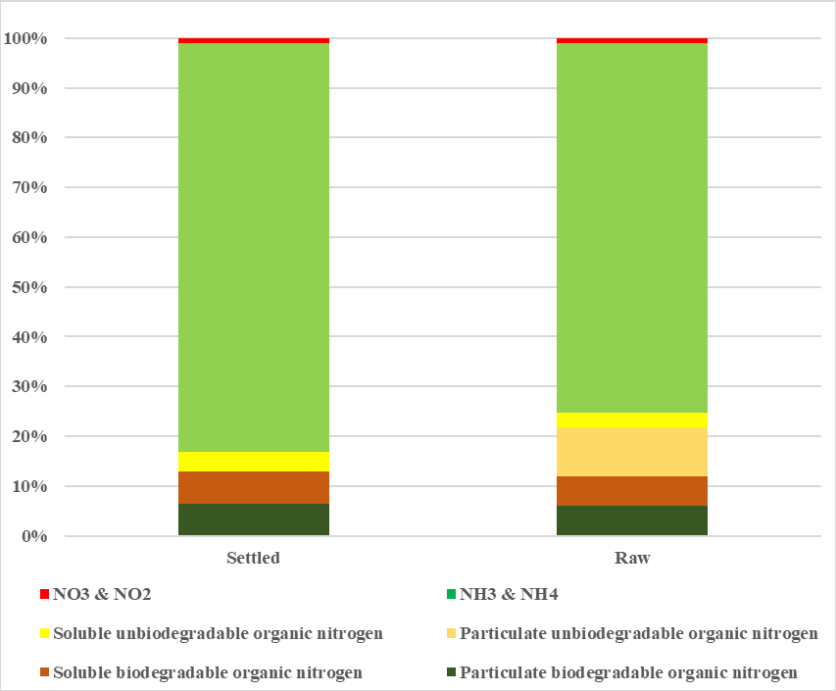

Figure 1.3: Classification of constituent fractions of total nitrogen in raw and settled wastewater(51)

The phosphorus compounds, which are mostly present in wastewater as phosphates, can be classified as phosphate compounds both physically i.e., dissolved or particulate fractions, and chemically. The chemical fractions are made up of organically bound phosphate, polyphosphate

or condensed phosphate, and dissolved inorganic orthophosphate (1). Phosphates are not harmful unless they are present at extremely high levels. However, high levels of contamination are mostly the result of extensive fertilizer use.

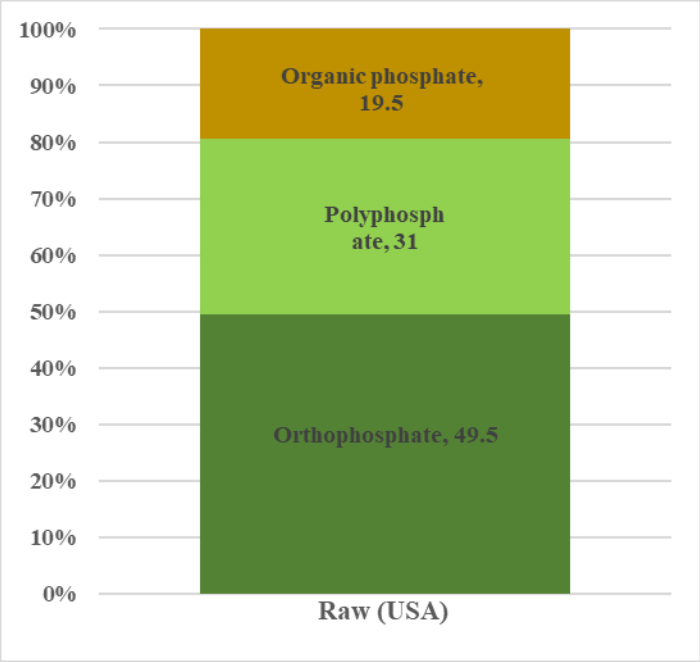

Figure 1.4: Classification of phosphorus in wastewater as a percentage of total phosphorus (51)

Although nitrate and phosphate anions are essential nutrients for living things, if their concentrations in water exceed the allowable limit, they can become contaminants. The eutrophication of water bodies is triggered by those extra nutrients (2). Therefore, before releasing polluted water into the environment, it must be treated to remove nutrients.

1.2 Objective

The objectives of the study are as follows:

- Performance Assessment of 3MLD SBR in terms of COD, NH_4-N, NO_3-N and PO_4-P removal.
- Synthesis of Graphene like biochar adsorbent from Agro waste.
- Characterization of Graphene like biochar adsorbent.

- Fabrication of Lab scale or demonstrated scale setup for the removal of additional nutrients from secondary treated effluent.
- Trial run and optimization of Graphene like biochar adsorption column setup.

1.3 Scope

The aim of this project is to evaluate the effectiveness of the synthesized Graphene like biochar adsorbent in removing COD and additional nutrients (NH_4-N, NO_3-N, and PO_4-P) from secondary treated effluent. Through this, we will be able to optimize the Graphene like biochar adsorption column setup.

Even though graphene is made from the inexpensive and widely accessible material, graphite, manufacturing is costly and limited. By eliminating volatile substances and raising the carbon content of the structure, the use of biomass waste can solve this issue while lowering the pollution it causes. This can be done through thermal processing, including low-temperature thermal processing, high-temperature pyrolysis including metal precursors, etc. One advancement in graphene technology may be seen in the creation of graphene by a green synthesis process. A variety of studies employ agricultural and other wastes as carbon source materials, including oil palm waste, rice husk, sugarcane bagasse, wheat straw, lignin, and animal byproducts.

CHAPTER 02

LITERATURE REVIEW

2.1 Introduction to nutrients

Excess levels of nitrogen and phosphorous in water can cause a phenomenon known as eutrophication, which can lead to the overgrowth of aquatic plants and algae. This can cause a depletion of oxygen in the water, resulting in the death of fish and other aquatic organisms. High levels of nitrogen and phosphorous can also lead to the formation of harmful algal blooms, which can produce toxins that can be harmful to humans and animals. Additionally, eutrophication can lead to the formation of dead zones in the water, where very little life can survive.

Nitrogen is a nutrient that can be found in various forms in water and wastewater, such as ammonia, nitrite, and nitrate. In natural water bodies, nitrogen is present in low levels and plays an important role in the ecosystem. However, when nitrogen levels become too high, it can lead to eutrophication, which can cause the overgrowth of aquatic plants and algae, resulting in a depletion of oxygen in the water, and the death of fish and other aquatic organisms.

In water treatment, nitrogen is typically removed from water through a process called denitrification. This process converts nitrogen compounds, such as nitrate and nitrite, into nitrogen gas, which is released into the atmosphere. Denitrification can be accomplished through a variety of methods, including the use of bacteria that consume the nitrogen compounds and convert them into nitrogen gas. Nitrogen in water and wastewater can be harmful but it can be removed by various methods such as chemical reduction and ion exchange, depending on the specific form of nitrogen present, the amount of nitrogen present, and the desired effluent water quality. It's important to note that the specific method chosen for nitrogen removal will depend on the type and concentration of nitrogen present in the water or wastewater, as well as the desired effluent water quality and discharge regulations.

Phosphorus is a nutrient that plays an important role in the growth of plants and algae. However, excess levels of phosphorus in water can lead to eutrophication, which can cause the overgrowth of aquatic plants and algae, resulting in a depletion of oxygen in the water, and the death of fish

and other aquatic organisms that's why various methods are used to remove phosphorus from water, including chemical precipitation, adsorption, biological phosphorus removal, and reverse osmosis, depending on the specific form of phosphorus present, the amount of phosphorus present, and the desired effluent water quality.

2.2 Overview of nutrient removal technologies

Nutrient pollution is the most common reason for poor water quality is the reason why, aquatic ecosystems are harmed by nutrient pollution, which has detrimental effects on the economy, a decline in biodiversity, and concern for human health. Nutrient pollution comes from a variety of sources, but contributions from human waste, such as wastewater and fecal sludge containing compounds of carbon, nitrogen, and phosphorus, are especially alarming (25). For this reason, phosphorus, nitrogen, carbon, and other micronutrients present in wastewater in wastewater treatment units should meet standard effluent limits for nutrients.

In general, chemical, physical, and biological approaches are used to remove nutrients from wastewater, however, chemical methods are less common due to their high cost, high sludge concentration, altered pH, and reduced settling capacity (27). When choosing treatment technology, there are additional considerations to consider, such as the solid handling capacity and current manual capability. In recent years, nitrogen and phosphorus removal technologies have been installed practically in all wastewater treatment facilities.

Floating materials, heavy settleable inorganic solids including grit, sand, and fats, oils, and grease are removed from wastewater as part of the preliminary treatment process. Large suspended particles are removed as the first step in treatment. Biological unit processes are used to carry out the secondary treatment. The biological oxygen demand of the effluent following secondary treatment is typically low and it may contain some dissolved oxygen. Tertiary treatment, also known as advanced treatment, refers to all procedures and techniques utilised to get rid of contaminants that weren't dealt with during conventional treatment. These pollutants could be microorganisms, remaining organic residue, dissolved and suspended particles such inorganic nitrogen and phosphorus compounds, etc.

In the early stages of the development of nutrient removal technologies, the first effort was made with the activated sludge process-based classical aerobic methods for the treatment of domestic wastewater. The broad application of these technologies, particularly in developing nations, is severely constrained by the high operational and capital expenses related to their deployment. Additionally, physical approaches have been shown to be too expensive due to the use of membranes, ineffective because they only remove around 10% of the total nutrients, and complicated further by membrane fouling. To effectively reduce the nutrient concentration of the effluent before releasing to surface waterways, nutrient removal through chemical dosing is also frequently used. However, the chemicals are expensive, handling and storing the chemicals is unsafe, and the approach produces more sludge, which drives up maintenance and operating costs. Biological nutrient removal technology is typically more economical than physical or chemical removal.

Table 2.1: A review of various technologies with their pollutant removal efficiencies.

S.No.	Type of technology/Material/adsorbent used	Pollutants removed	Efficiency	Reference
1	Nitrification and denitrification	Organics and nutrients	50-70%	(23)
2	Advanced oxidation processes (Hydroxyl radical)	Nitrogen	>95%.	(24)
3	Chemical precipitation	Nitrogen	20–30%	(24)
4	Xylem filter	Bacteria	99.9	(25)
5	Reduced Graphene Oxide (RGO)	Methylene blue Copper (II) ions	97.2% 99.5%	(27)
6	Graphene oxide nanoplatelets	Safranin dye	97.78%	(26)
7	Graphene oxide nanoplatelets	Crystal violet	90–99.8%	(27)

8	Polonite adsorbent Wetlands process Ion exchange media (zeolite) Enhanced biological Phosphorous removal MBR Granular sludge reactors Sequencing batch biofilm reactors Membrane Aerated Biofilm Reactors Microalgal biofilm photobioreactors	Phosphorous	91% 40-60% 80–90% 88% 53% 87% 50% 90% 97%	(28)
9	Single-tank sludge treatment	TN PO_4-P	88% 87%	(29)
10	Biological treatment with activated sludge process	Phosphate-ion Ammonium-ion	97.8% 99.5%	(26)
11	Air stripping Membrane separation Biological assimilation	Total Nitrogen	70-92% 99-100% 83-87%	(26)
12	Intermittent cycle moving bed biofilm reactor (ICMBBR)	TN TP TKN NH_4-N TKN	91.8% 88.95% 92.8% 93.3% 92%	(30)

(31) studied the performance of the adsorption capacity of chitosan and activated charcoal has been scrutinized using a UV–Vis spectrophotometer. Both chitosan and activated charcoal has been studied for their ability to absorb nitrate and phosphate anions from water/wastewater by varying various parameters like pH, initial concentration, contact time, and adsorbent dosage. The adsorption capacity of chitosan was found to be better than activated charcoal. Therefore, it was

concluded by the author that chitosan is a less expensive, more biocompatible, and more effective adsorbent for removing nitrate and phosphate ions from water samples. (32) presented the techniques and significant findings regarding nitrogen and phosphorus recovery from wastewater. It includes methods based on physical, chemical, and biological principles. Future studies are required to integrate fundamental knowledge with technological adaptation for a specific site/wastewater. (33) studied the comparison of the various techniques, while considering the expenses and efficiency, as well as the procedures employed for the removal of nitrogen, phosphorous, and their compounds. The author also discusses the ultimate disposal of the removed contaminants.

2.3 Biological nutrient removal treatment

The term "biological nutrient removal" refers to Activated Sludge Process variants that use microorganisms in aerobic, anaerobic, and anoxic environments to remove Total Nitrogen, Total Phosphorous, and Chemical Oxygen Demand through metabolic processes such as nitrification, denitrification, and biological phosphorus removal. Biological nutrient removal is subject to a wide range of conditions and factors, including nutrient ratios, loading rates, waste rates, dissolved oxygen, and retention durations, among others (23).

a) Biological nitrogen removal: In recent years, biological nitrogen removal techniques have become more popular. Nitrification occurs in the aerobic media first, followed by denitrification in the anoxic medium, in the traditional biological nitrogen removal process. The most popular and economical approach for removing nitrogen from wastewater is biological nitrogen removal. In many instances, it aids in achieving the desired effluent Total Nitrogen. First, under aerobic conditions, autotrophic bacteria oxidise ammonium and nitrite to produce nitrate or nitrification; next, under anoxic conditions, heterotrophic microorganisms decrease nitrate to produce nitrogen gas or denitrification. Suspended growth systems, such as the Modified Ludzck Ettinger, four-stage Bardenpho process, oxidation ditches, Sequencing Batch Reactors, and others, are the most often utilised system modifications at WWTPs. Attached growth and hybrid systems are also employed. When both aerobic and anoxic zones are present, as in oxidation ditches and membrane-aerated biofilm reactors, nitrification and denitrification can take place sequentially or simultaneously.

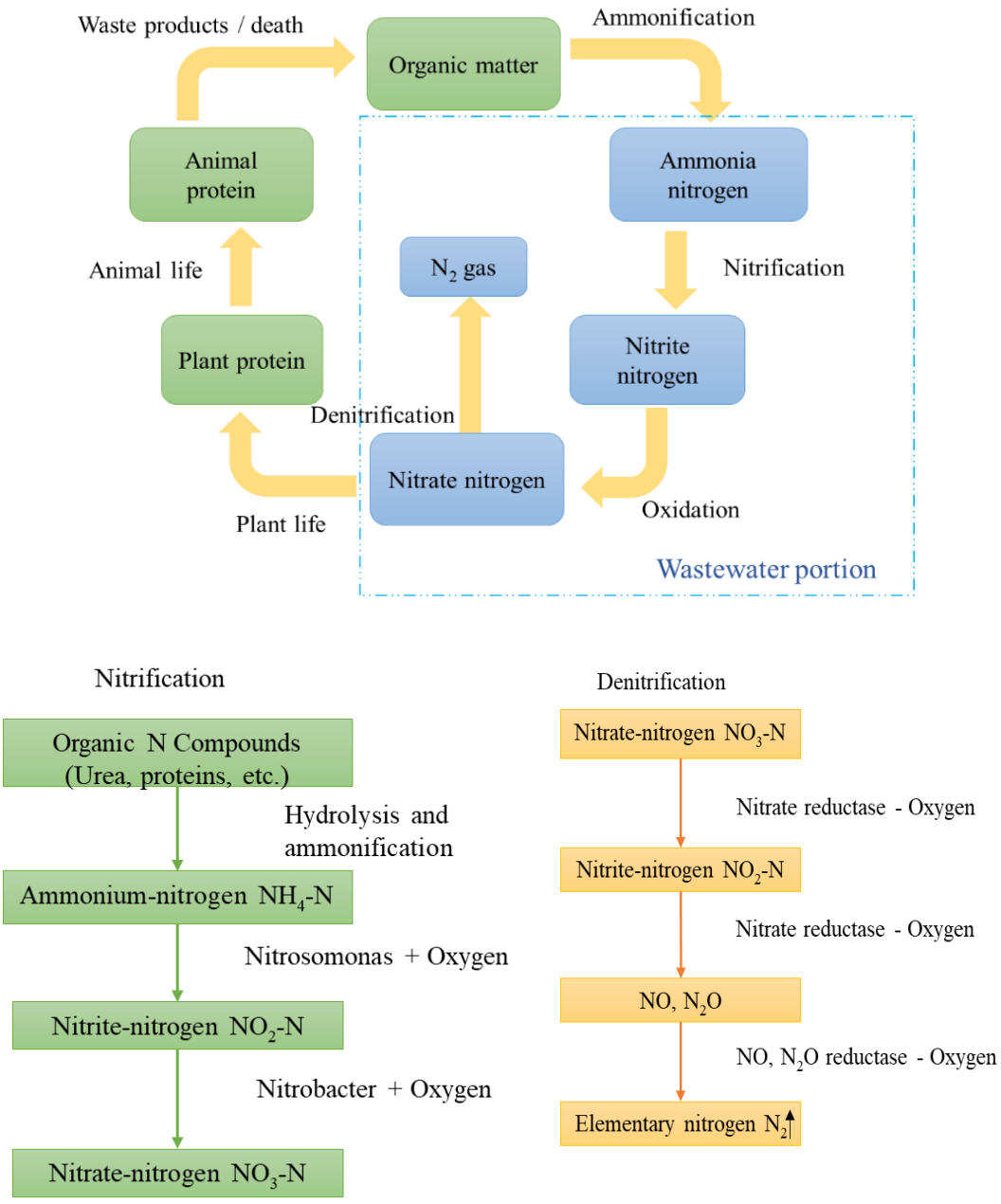

Figure 2.1: Nitrogen Cycle with degradation processes of Nitrification and Denitrification

The two-step autotrophic reactions that make up the nitrification process include the conversion of ammonium to nitrite and the subsequent oxidation of nitrite to nitrate in the presence of oxygen. Ammonia-oxidizing bacteria like Nitrosomonas, Nitrosococcus, and Nitrosospira carry out the first step's oxidation of ammonia/ammonium to nitrite, which results in the following reaction: (24)

$NH_3 + O_2$ + Alkalinity + Nitrosomonas = NO_2

Nitrobacter, Nitrospira, and Nitrococcus in particular, which are nitrite-oxidizing microbes, convert nitrite to nitrate in the usual sequence, causing the following reaction:

$NO_2 + O_2$ + Alkalinity + Nitrobacter = NO_3

The BNR process' effectiveness is dependent on the growth and activity of the bacteria, which are susceptible to changes in parameters including temperature, pH, alkalinity, DO, C/N ratio, solids retention time, inorganic metals, and others (25).

a) Biological phosphorus removal: Enhanced Biological Phosphorous Removal removes phosphorus from activated sludge using heterotrophic bacteria called Phosphorus accumulating organisms which have a high affinity for ingesting and storing Phosphorus. In the anaerobic phase, phosphorus-accumulating organisms release Phosphorus, which those same phosphorus-accumulating organisms then take up in the aerobic phase. Phosphorus is taken out of the influent and put into biomass. When compared to chemical treatment for home wastewater, it is one of the most affordable environmentally sustainable options. By uptaking polyphosphate, orthophosphate, and organically bound phosphorus into cell biomass and then desludging the biomass from the treatment unit, biological phosphorus removal from wastewater is accomplished.

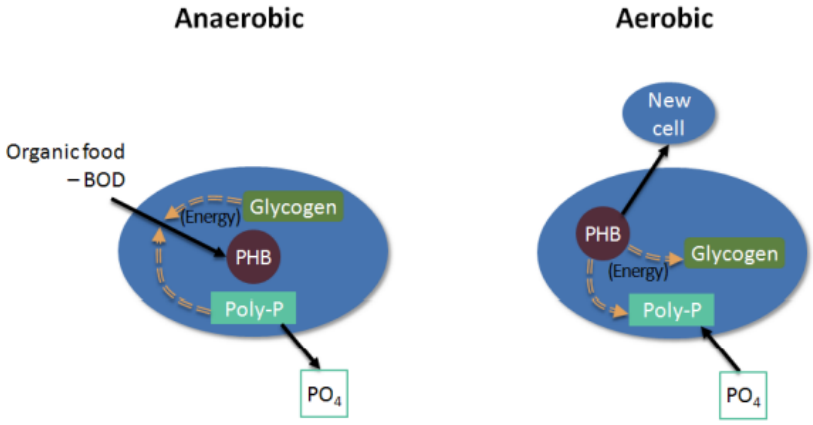

Figure 2.2: Mechanism of p removal (28)

Biological nutrient removal technology needs higher standards of operator skill and consideration, wider use of the research facility, and more serious cycle checking and change. To get the desired effluent TN, it can require on external carbon sources or energy input. In addition, it requires big footprints, has a slow reaction time, and other characteristics that make funding difficult. The Biological nutrient removal process also has other drawbacks, including difficulties with sludge settleability, the requirement for large reactors, settling tanks, biomass recycling, slow reaction rates (24).

2.4 Chemical Precipitation

Salts containing nutrients are precipitated by adding chemicals to wastewater. Both N and P are frequently present in precipitated salts, but P is usually eliminated in higher amounts. Chemical precipitation, frequently using calcium, aluminium, or iron, can be the quickest and absolute cheapest approach to remove excess dissolved phosphorus from wastewater effluent. Chemical precipitation is the transformation of elements dissolved in water into solid particles during the treatment of wastewater (24). When using chemical precipitation, alkalinity, pH, and hardness are three important things to consider.

Magnesium salts are the most usual additive for crystallisation procedures; aluminium and iron salts are the most widely used additives2 and can attain effluent concentrations of 0.3-0.5 mg/L Total phosphorus. Although many additional configurations are available, the primary clarifier effluent or the sludge treatment process are frequently supplemented with chemicals. Nutrient-rich biosolids or crystallised materials like struvite, brushite, or calcium phosphate are examples of process by-products. Different byproducts have different values; some are better fertilisers than others. The method has advantages such as inexpensive initial investment and ease of operation, but the operating expenses are significant because chemicals are used, energy is expensive, and the precipitated sludge that is produced must be disposed of. Operations can be complicated, and good operations require upstream treatment processes. Phosphorous- rich chemical recovery from sludge might be difficult.

2.5 Reverse osmosis

Using a selectively permeable membrane, reverse osmosis is a technique used to extract dissolved solids from wastewater. A high-pressure pump drives water molecule through a permeable membrane to separate wastewater streams into discharge-continuous permeate and concentrate streams. The fact that the primary equipment used in the Reverse Osmosis process is simple to use, compact, and easy to maintain under control is one of its benefits. The apparatus is also flexible, allowing it to be scaled up or used in confined spaces. Based on the operating circumstances, the method has been shown to eliminate all bacteria, up to 99% of inorganic ions, and more than 99% of the organic macromolecules from wastewater. It is a procedure that is economically viable.

The concentration produced by nitrogen removal via Reverse Osmosis membrane separation is quite large and needs additional processing. Because Reverse Osmosis membranes can't effectively handle feed water that contains suspended solids, pre-treatment separation operations must in some way stop solids from transferring to the membrane system. Membrane fouling, which reduces the treatment's effectiveness and concentrates output, is a further drawback of using RO to treat wastewater (24).

2.6 Breakpoint chlorination

Adding chlorine or hypochlorite direct to the wastewater is known as breakpoint chlorination. Chloramines are created when ammonia and chlorine react (26). The pH affects the type of chloramine that is produced. Chlorine added in excess causes the "breakpoint" to change from chloramines to nitrogen gas. Chlorine overdose increases the amount of free chlorine in effluent, creating breakpoints.

Breakpoint chlorination has the advantages of being able to completely oxidise ammonia and having a straightforward application technique. Furthermore, reaction variables like temperature and hazardous chemicals are not independent of the process. But because it cannot be used to treat wastewater with a high concentration of NH_4^+-N, this approach can only be used as an advanced treatment. Due to the formation of halogenated organic compounds like chloramines, which can be hazardous to both aquatic life and human health, environmental contamination is also a big concern with this process. The cost of using this approach is substantial.

2.7 Ion exchange

Ion exchange is a unit process in which solution-derived ions of various species displace ions of a particular species from an insoluble exchange medium. In practice, the waste to be treated is passed through an ion exchange resin that has been set up in a bed. A regenerative solution is delivered through the bed when the feed is terminated once the exchange capacity of the bed has been used up. Depending on the chemical makeup of the wastewater to be treated and the final destination of the contaminants, the anion exchange method may be used to remove nitrogen and phosphorus (26). Desalination and deionization of water both utilize ion exchange technology. The advantage of ion exchange systems is that they can achieve phosphorous recovery by post-treating the sorption medium. Ion exchange is the process by which ions on a solid's surface trade places with ions present in a solution to which the solid is subjected. Numerous variables, including pH, temperature, particle size, initial nutrient concentration, contact time, and adsorbent dosage, influence the removal of nutrients. The ion exchange process has various benefits, including the capacity to remove organic materials and heavy metals from wastewater, minimal costs, and good stability. Ion exchangers and adsorbents, however, have a very short lifespan and must be replaced frequently, creating extra waste that needs additional treatment and disposal.

2.8 Air stripping

When wastewater is exposed to air, volatile compounds that are present in the wastewater are released and taken up by the air in gaseous form. This process is known as "air stripping." The procedure increases the exchange of the pollutant from the fluid stage to the vaporous stage by generating a situation in which a large surface area of wastewater is exposed to the air. The effectiveness of stripping is influenced by many variables, including temperature, pH, the length of the stripping process, and the volume ratio of air to liquid. Poor stripping performance is caused by the problem of fouling, which happens when calcium carbonate scale forms on the packing equipment's surface. High sludge production and alkaline effluent are also linked to the air stripping process, which increases cost and treatment. Environmental pollution arises from the stripping process's discharge of ammonia gas into the atmosphere. Nitrogen removal has traditionally been done by air-stripping ammonia. The procedure is carried out in a packed tower because it offers a sizable mass transfer area and has a high stripping efficiency (22).

2.9 Adsorption

A number of pollutants can be eliminated from wastewater using the purification method known as adsorption. Adsorption is a process by which a concentrated version of the adsorbate, usually as a gas or liquid, adheres to the surface or pores of a solid adsorbent. The effectiveness of the adsorbent influences whether the adsorption process is successful or unsuccessful. In comparison to other treatment techniques, the adsorption process has several benefits, including high removal effectiveness, cheap cost, ease of application, minimal sensitivity to pH and temperature, and environmental friendliness. The amount of ammonium removed by the adsorption process is significantly influenced by pH. Because there are less ammonia ions in alkaline settings, the effectiveness of ammonium removal decreases as pH increases. The table below illustrates two different types of adsorption processes: physical adsorption and chemical adsorption. If the attraction forces between the adsorbent and the adsorbate are Vander Waal forces, then physical adsorption occurs. Assuming that the force of attraction between the adsorbate and the adsorbent is about equal to the strength of chemical bonds, chemical adsorption takes place. Adsorption by chemicals is a permanent process. The creation of inexpensive adsorbents with the best ability to extract contaminants from wastewater, such as natural materials, agricultural wastes, and industrial wastes, has been the focus of a recent study.

CHAPTER 03

MATERIAL AND METHOD

3.1 Biochar adsorbent preparation

Sugarcane bagasse was collected from the sugar mills, and then it was cut into small pieces and washed thoroughly with deionized water several times to remove the impurities. It was then dried in the sunlight for a few days. After being sun-dried, it was dried at 70℃ in a vacuum oven for 24 hrs. The material was triturated to a fine powder and subjected to pyrolysis at 550℃ for 1 hr. 15 min, 1 hr., 45 min., and 30 min. in the presence of Nitrogen gas. The resultant powder was ground further and then washed with 2 M of nitric acid to remove by-products. The final product was filtered and washed with warm deionized water several times and then oven-dried for 24 hrs. The resultant adsorbent was ultrasonicated at Time - 30 min; Temp - 30℃; Pulse- 20 05; and Ampl – 40%.

Figure 3.1: a) Sugarcane bagasse being dried in sunlight. b) Sugarcane bagasse being Vacuum oven dried at 70℃. c) Grinding of oven-dried sugarcane bagasse. d) Pyrolysis equipment setup. e) Resultant black powder obtained after Pyrolysis. f) Ground Resultant black powder. g) Washing and Filtering of Resultant black powder.

3.2 Adsorbate

The treated effluent from the 3MLD Sequencing Batch Reactor sewage treatment plant located at Solani Kunj near the C-class club at the IIT Roorkee campus was used as the adsorbate for the column setup. The SBR system is the foundation of the STP. In order to achieve biological treatment and sedimentation in the same basin, it employs a fill-and-draw cyclical approach with both aeration and non-aeration sequencing. The deodourization system for further odour control for sump wells and pre-treatment units, and the advanced tertiary treatment facility (Fibre Disc filtration and UV as well as chlorine dosing for disinfection) are the key components of this established STP (4).

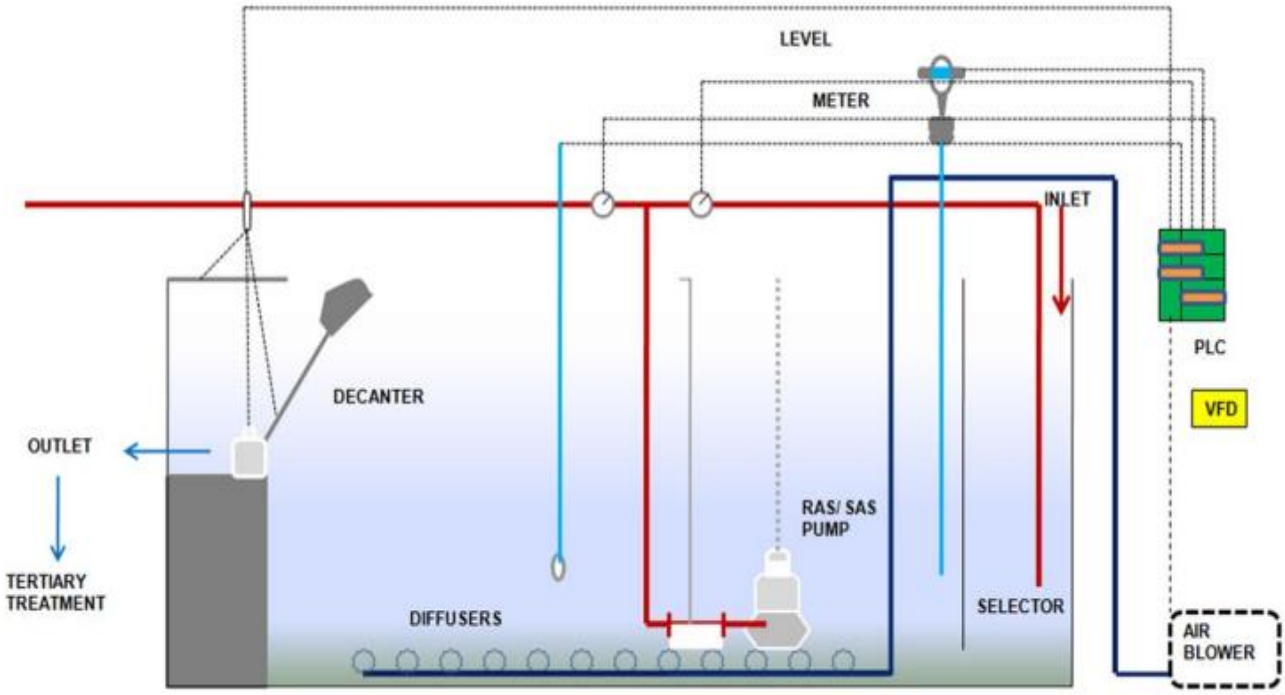

Figure 3.2: Schematic Layout of 3MLD STP (4)

3.3 Column study experimental details

The Experimental column setup shown in the figure below was used for the dynamic column studies. It consists of 4 columns made of borosilicate glass with an internal diameter of 30 mm and a length of 250 mm. All 04 columns were packed with the different adsorbent materials (35 mm) varying in preparation time viz. 30 min., 45 min., 1 hr., and 1 hr. 15 min. respectively between the

supporting layers of glass wool (10 mm) each (for improving the flow distribution and prevention of the loss of adsorbent (6)), and gravel (105mm and 90 mm). The Peristaltic pump RH-P100L-100-4R was used to draw water from the inlet water can to the column. The up-flow mode was used to prevent channeling and assure consistent streaming. Before starting the experiment, the filter was fed with distilled water for some time to remove impurities from the absorbent.

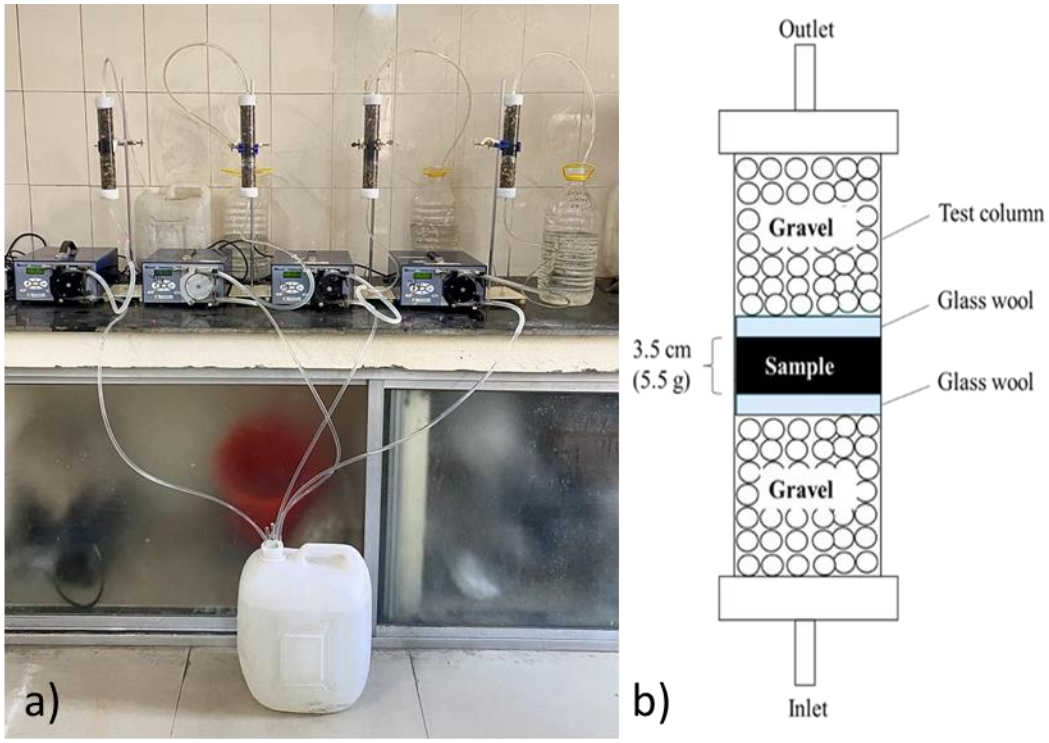

Figure 3.3: a) Column setup b) Column packing

3.4 Mathematical models

The "effluent concentration-time" profile, often known as the breakthrough curve, is used to characterise the dynamic behaviour of continuous adsorption columns (35). It is necessary to use mathematical models to represent and correlate the experimental breakthrough curve data while designing and optimising adsorption columns (36). The experiment results in breakthrough curves and the estimation of some kinetic coefficients are frequently described using the Thomas model, Yoon-Nelson model, and Bohart-Adams model (34).

3.4.1 Thomas Model

One of the most general and commonly applied models in continuous column adsorption performance theory is the Thomas model. It is produced on the assumption that the adsorption process shows a pseudo-second-order kinetics and Langmuir isotherm with no axial dispersion in the adsorption column. (36). The main drawback is that its derivation is based on second-order kinetics and assumes that sorption is regulated by mass transfer at the interface rather than the chemical reaction, which limits sorption (35). The following expression may be used to describe this model's linearized form:

$$\ln\left[\frac{C_i}{C_f} - 1\right] = \frac{k_{TH} q_0 w}{Q} - k_{TH} C_i t \qquad (1)$$

Where,

C_i = influent concentration (mg L^{-1})

C_f = effluent concentration (mg L^{-1})

k_{TH} = thomas rate constant (ml min^{-1} mg^{-1})

q_0 = maximum solid-phase concentration of solute or adsorption capacity (mg g^{-1})

w = mass of the adsorbent in column (g)

Q = the flow rate (ml min^{-1})

t = total flow time (min)

3.4.2 Adams-Bohart Model

The basic equation, which defines the relationship between C_f / C_i and t in a continuous system, was developed by Adams and Bohart. The Adams-Bohart model offers a straightforward and all-inclusive method for carrying out and analysing sorption-column tests. The assumption of a negligible mass transfer or axial dispersion makes the adsorption rate advantageous, dependent on the residual capacity of the adsorbent and the concentration of the adsorbed species (35). The breakthrough curve's beginning is mostly described using the model. It can be expressed by following expression

$$\ln\left[\frac{C_i}{C_f} - 1\right] = k_{AB}N_0\frac{z}{u} - k_{AB}C_i t \quad (2)$$

Where,

C_i = influent concentration (mg L^{-1})

C_f = effluent concentration (mg L^{-1})

k_{AB} = kinetic constant (ml min^{-1} mg^{-1})

N_0 = sorption capacity (mg L^{-1})

z = bed-depth (cm)

u = linear velocity (mmh^{-1})

t = total flow time (min)

3.4.3 Yoon Nelson Model

The Yoon-Nelson model is a very straightforward breakthrough model that assumes that the chance of each molecule adsorbing at a given rate is inversely proportional to the probability of adsorbate adsorption and breakthrough inside the bed (36). This model is less complex and does not require specific details on the sorbate's properties, the kind of adsorbent, or the sorption bed's physical parameters. It can be expressed by following expression

$$\ln\left[\frac{c_f}{c_i - c_f}\right] = k_{YN}t - \tau k_{YN} \quad (3)$$

Where,

C_i = influent concentration (mg L^{-1})

C_f = effluent concentration (mg L^{-1})

k_{YN} = rate constant (ml min^{-1} mg^{-1})

τ = time required for 50% sorbate breakthrough

t = total flow time (min)

3.5 Characterization of adsorbent

In order to provide a more accurate interpretation of the mechanism at play during the adsorption process, the adsorbent was characterised with the goal of evaluating its numerous physical and chemical properties (5). The surface morphology in the adsorbent was visualized by using scanning electron microscopy (SEM) with Scanning Tunneling Electron Microscope with magnifications 12- 200,000X (SE) and 100- 100,000X (BSE). The SEM's energy dispersive X-ray (EDX) instrument was used to conduct the EDX. A diffractometer with 2.2 kW Cu radiation running at 40 kV with 40 mA was utilised to record the X-ray Diffraction (XRD) patterns, and the 2 theta values investigated varied from 5 to 120º. The vibration frequency variations in the functional groups of the carbons were measured using Fourier transform infrared spectroscopy (FTIR) (5). A Thermo Nicolet Nexus FTIR spectrophotometer was used to measure the carbons' spectra in the 400–4000 cm^{-1} wavenumber region. Raman measurements were performed using a Raman spectrometer with the serial number 021R88 that is outfitted with a CCD detector, 50x objective lens, and an argon ion laser as the source of excitation.

CHAPTER 04

RESULTS AND DISCUSSION

4.1 Characterization of adsorbent

4.1.1 Scanning Electron Microscopy and Electron Dispersive X-ray Analysis

The surface morphological characteristics of the adsorbent made from sugarcane bagasse at 550°C were examined in this work using FE-SEM (Zeiss GeminiSEM) and EDX. Samples were initially coated with a 9 nm gold coating using a sputter coater for FE-SEM analysis in order to reduce sample charging due to non-conducting materials. The binary images are segmented into black and white regions that represent solid surfaces and void spaces, respectively, to identify the microporous regions (7). FE-SEM images of all adsorbent samples produced at 550°C varying in preparation time viz. 30 min., 45 min., 1 hr., and 1 hr. 15 min. are shown below in Figure 1a,1b,1c and 1d, respectively. EDX analysis results are shown in Figure 2, where the results are presented in the weight percentage of all 04 samples. EDX of these samples detects Carbon (78.26% for sample 01, 77.85% for sample 02, 76.26% for sample 03, and 77.34% for sample 04), Oxygen (21.13% for sample 01, 21.06% for sample 02, 22.99% for sample 03 and 21.91% for sample 04), and some amount of minerals such as silicon (0.61% for sample 01, 1.09% for sample 02, 0.76% for sample 03 and 0.75% for sample 04) and gold. As a result of the gold coating used to charge each sample prior to the examination and the sample's non-conducting nature, it is evident that each sample contains some gold. These findings showed that carbon was the primary skeleton in all of the 04 adsorbent samples, with oxygen present in functional groups (such as -COOH and -OH) or metal mineral particles (e.g., carbonate, phosphate, and sulfate) (8). Generally, all adsorbents had porous meso and micropore and honeycomb structures. SEM image observation of all samples also showed the structure of the graphene layers formation along the structure (9).

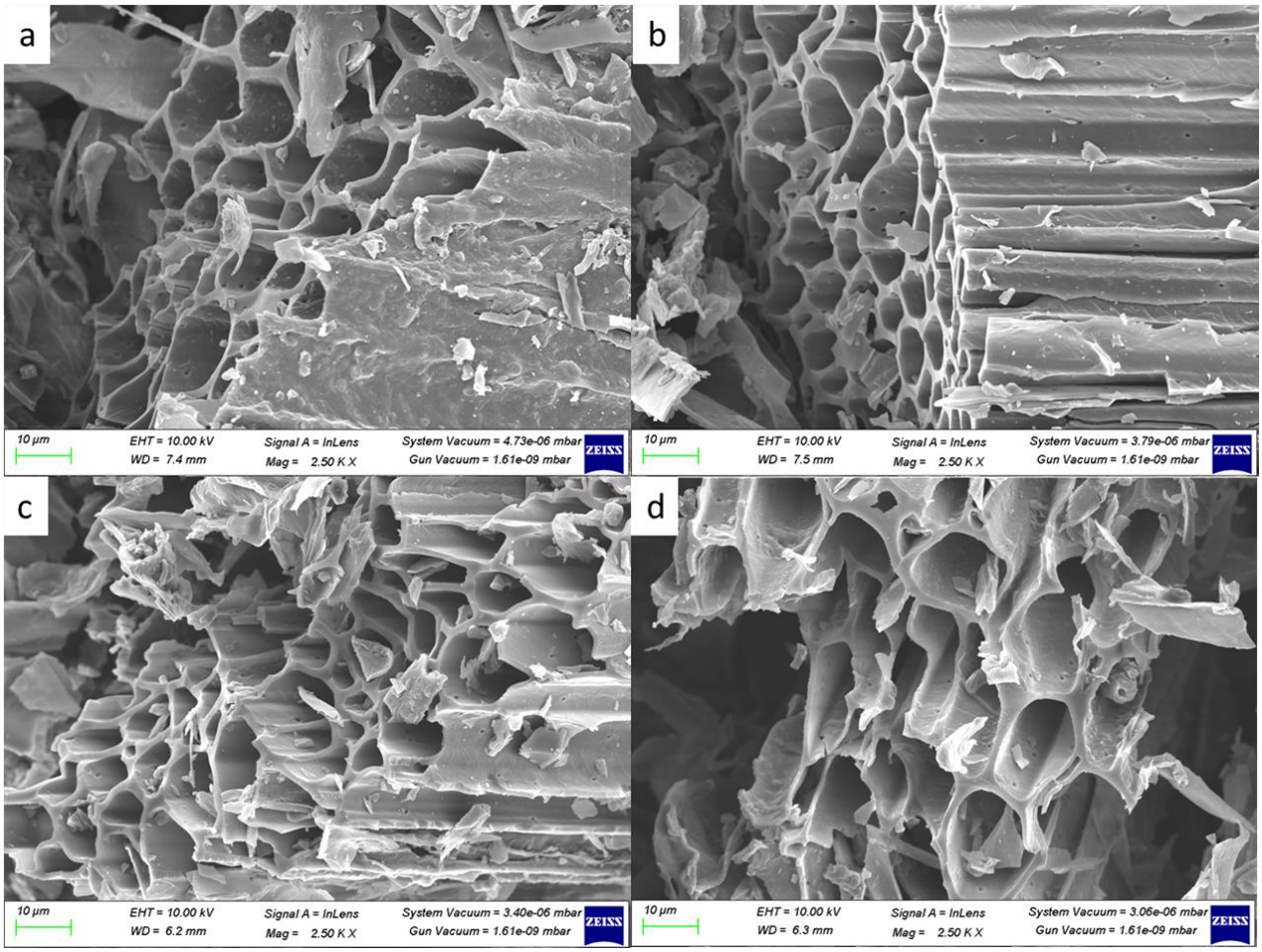

Figure 4.1: SEM for all 04 samples

Table 4.1: EDX analysis results for Sample 01

Element	Weight Percentage	Atomic Percentage
C	78.26	82.92
O	21.13	16.80
Si	0.61	0.28
Total:	100.00	100.00

Table 4.2: EDX analysis results for Sample 02

Element	Weight Percentage	Atomic Percentage
C	77.85	82.71
O	21.06	16.80
Si	1.09	0.50
Total:	100.00	100.00

Table 4.3: EDX analysis results for Sample 03

Element	Weight Percentage	Atomic Percentage
C	76.26	81.26
O	22.99	18.39
Si	0.76	0.35
Total:	100.00	100.00

Table 4.4: EDX analysis results for Sample 04

Element	Weight Percentage	Atomic Percentage
C	77.34	82.18
O	21.91	17.48
Si	0.75	0.34
Total:	100.00	100.00

4.1.2 Fourier Transform Infrared Spectroscopy

The vibration frequency variations in the functional groups of the carbons were measured using Fourier transform infrared spectroscopy (FTIR) (5). A Thermo Nicolet Nexus FTIR spectrophotometer was used to measure the carbons' spectra in the 400–4000 cm^{-1} wavenumber region. As indicated in the figure below, spectra were plotted for the adsorbents using the same scale on the transmittance axis. The O-H stretching vibrations of the C-OH groups and water are responsible for the prominent peak centered at 3427, 3449, 3442, and 3454 cm^{1} for all 04 samples, respectively (12,13). It is significant to note that the oxygen content in the samples has a direct correlation with the intensity of the wide peak associated with the C-OH stretching vibration, which results in hydrogen bonding between Graphene Oxide layers and between GO and water molecules, creating, the hydrophilic moiety of the sample (11). The adsorption band was attributed to C=O stretching at a wavelength of 1614,1631, 1626, and 1629 cm^{-1} for all the samples, respectively. The strongest bands in the spectra of samples were found at 3420-3460 cm^{-1}, in the fingerprint area, and were attributed to C-OH stretching (9). While examining the spectrum of all the samples, certain peaks roughly at 1180, 600, and 470 cm^{-1} could be clearly recognised. These peaks were attributed to the carbon silicon (14,15).

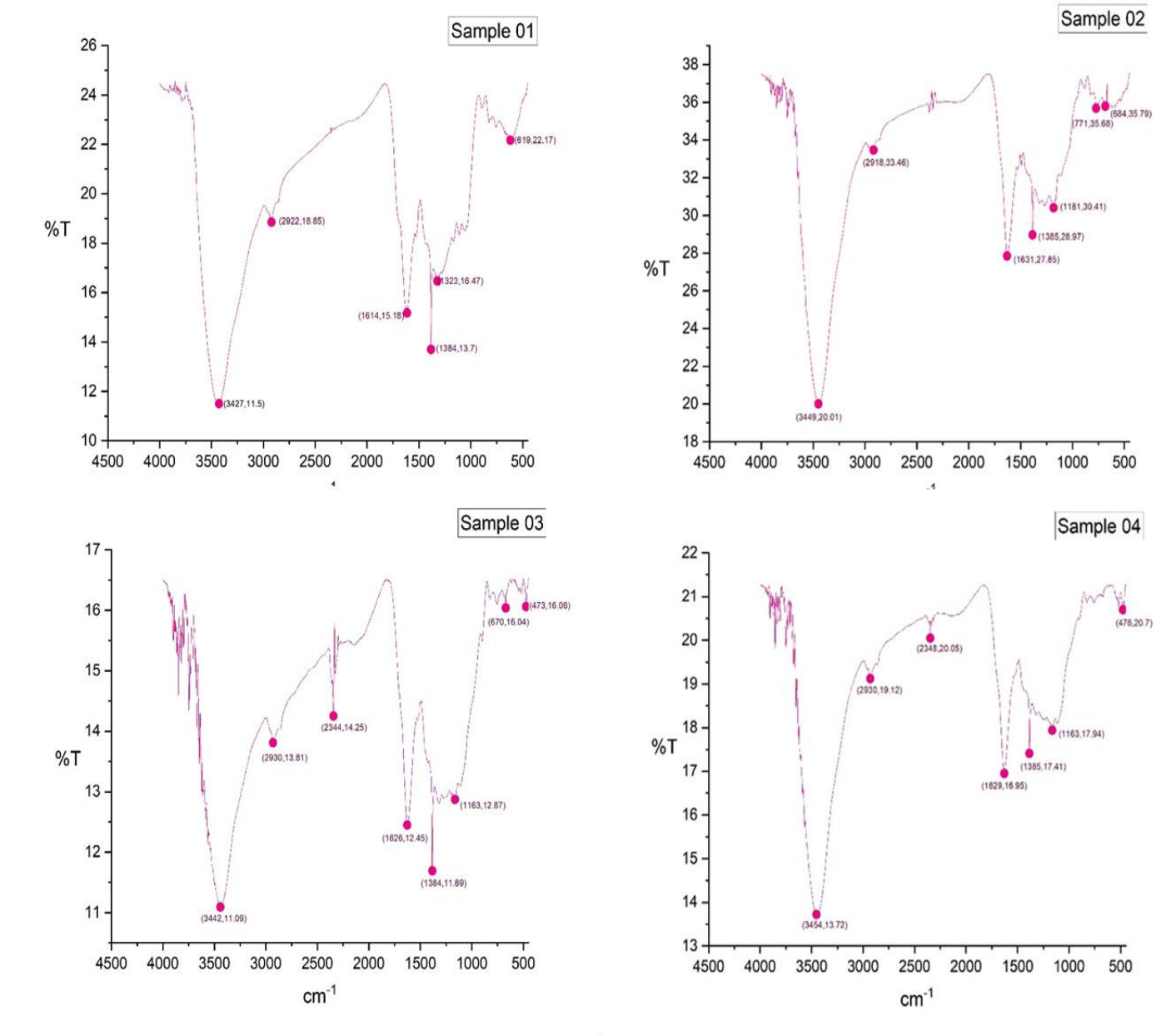

Figure 4.2.: FTIR for all 04 samples

4.1.3 Raman Spectroscopy

Using an argon ion laser as the source of excitation, measurements of the Raman spectrum were performed using a Raman spectrometer (series no. 021R88) with a CCD detector and 50x objective lens. The existence of the G-bands, which result from the graphitic hexagon-pinch mode's stretching of sp^2 carbon, can be seen clearly in the figure below. For samples 01, 02, 03, and 04 the G-band is at 1602, 1599, 1597, and 1595cm^{-1}. Impurities and edges, which cause atomic arrangement disorder, are the cause of the D-appearance bands. The distinctive D-bands, which result from bending the sp^3 carbons in graphene sheets, are situated at 1364, 1365, 1346, and 1371 for samples 01, 02, 03 and 04, respectively (9). Raman spectroscopy revealed two primary peaks at the D band and G band, which, respectively, represented the edge of the graphene layer and a perfect lattice of carbon. In an aromatic molecule that corresponds to the amorphous state of the benzene ring, both peaks demonstrated the presence of carbon atoms (10). The 2D band is the second strongest feature in the Raman spectrum of graphene and is associated with the out-of-plane vibrational mode of the carbon atoms. The 2D band is typically located roughly at 2700 cm^{-1} for all the samples.

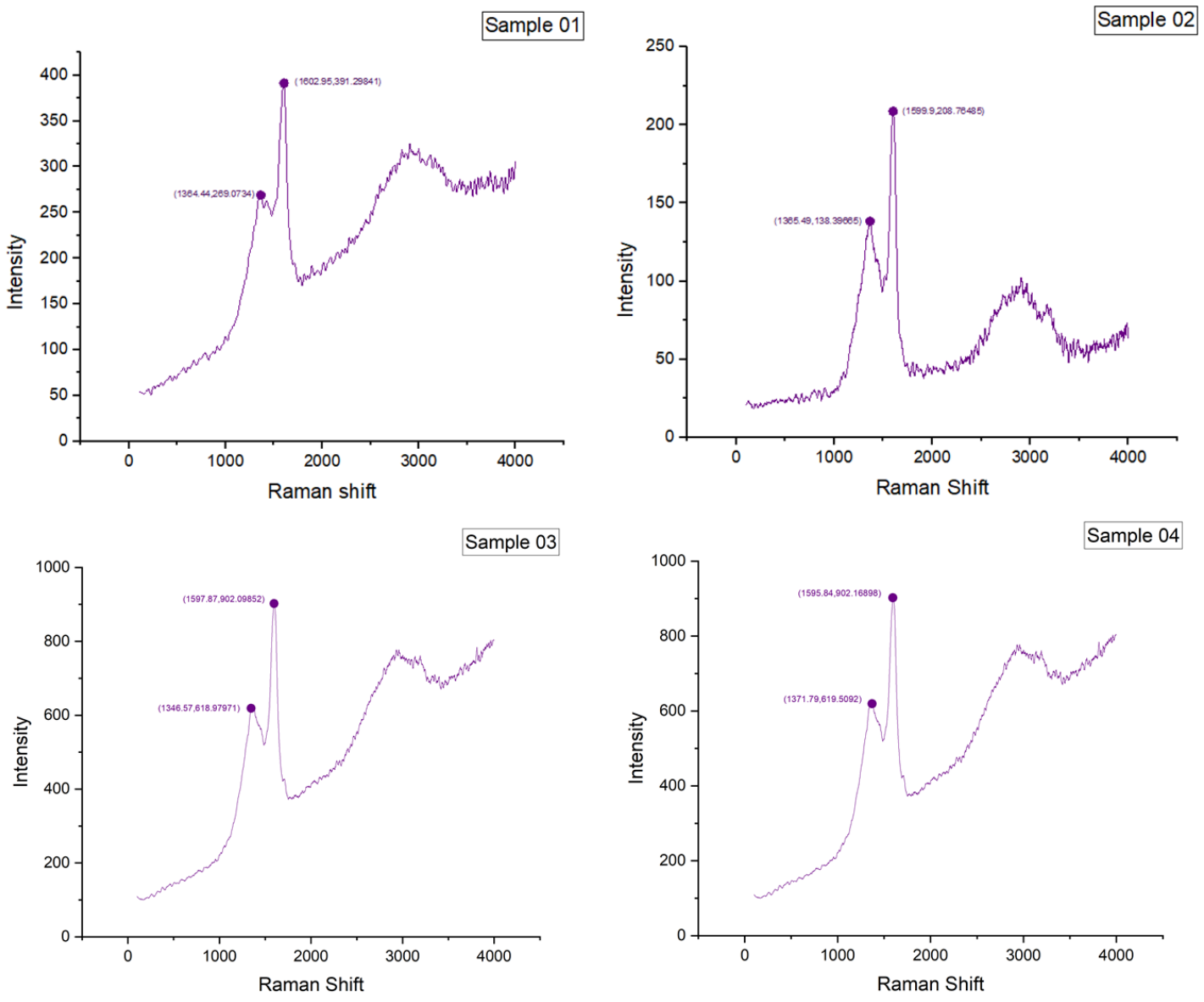

Figure 5.3: Raman for all 04 samples

4.1.4 X-ray Diffraction

A diffractometer with 2.2 kW Cu radiation running at 40 kV with 40 mA was utilised to record the X-ray Diffraction (XRD) patterns, and the 2 theta values investigated varied from 5 to 120º. The absence of a peak indicating the formation of the crystal phase and the two broad peaks roughly at 2Θ= 22° and 2 Θ = 26° suggest that all the samples were amorphous carbon. The

position and intensity of this peak from the figure below provides information about the degree of graphitization in the biochar sample. When materials originating from agricultural byproducts are pyrolyzed, graphene structures can emerge (16).

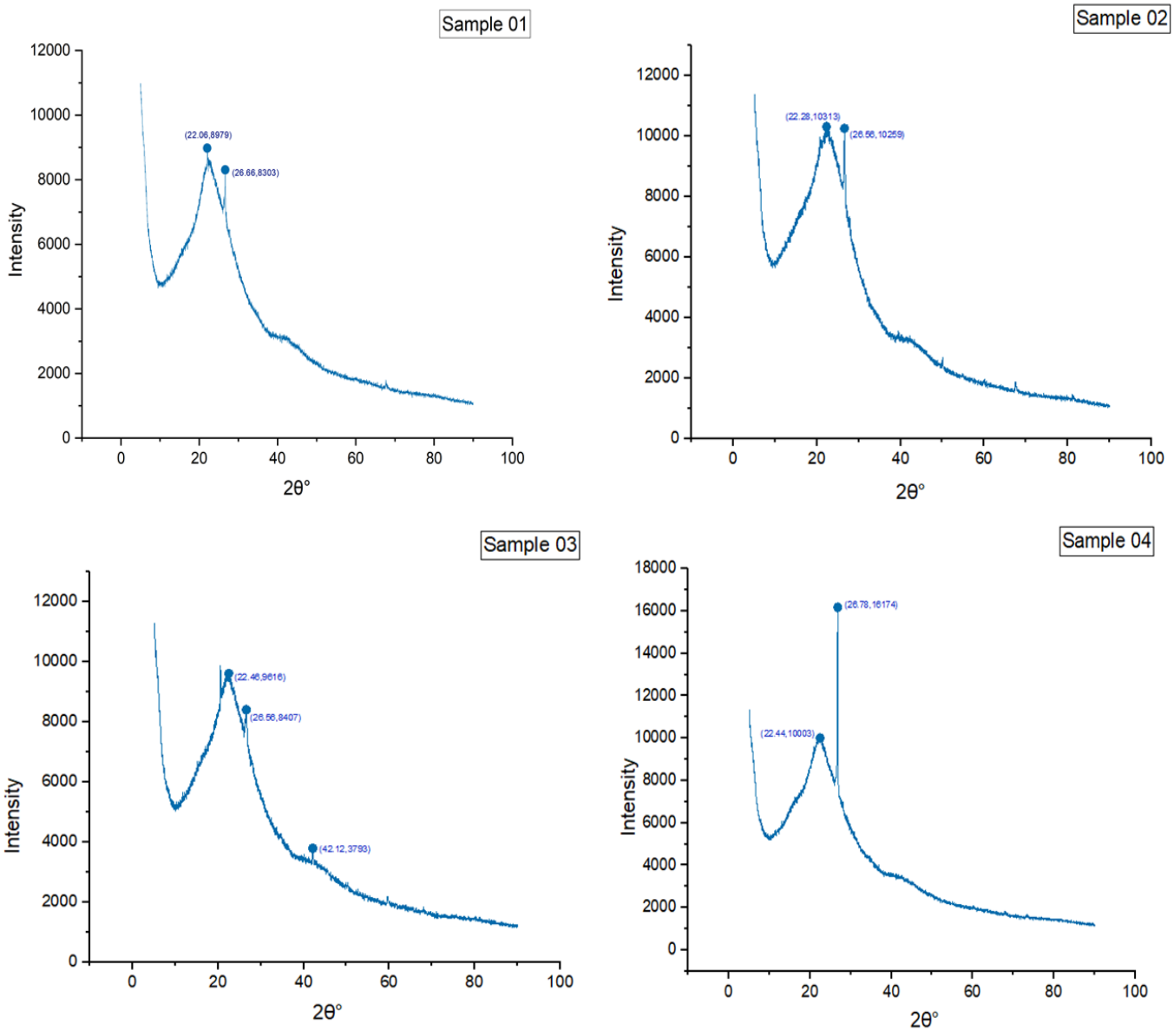

Figure 5.4: XRD for all 04 samples

4.1.5 Surface area measurement

The pore volume, pore size and BET surface area of all four samples were determined using the ASAP 2020 Micromeritics surface area analyzer which is illustrated in table below. According to the IUPAC, there are three types of porous structure: micropore (diameter < 2 nm), mesopore (diameter 2– 50 nm), and macropore (diameter > 50 nm).

Table 4.5: BET surface and pore volume of all 04 samples.

Sample	BET surface area (m^2/g)	Mean pore diameter (mm)	Total pore Volume (cm^3/g)
Sample 01	60.2	2.0	0.07
Sample 02	60.1	2.1	0.06
Sample 03	60.3	2.2	0.09
Sample 04	59.9	2.3	0.08

4.2 Performance evaluation of 3MLD SBR Plant at IIT Roorkee campus

Table 4.5 displays the appraisal of STP's overall performance. A full-scale plant designed to process 3.2 million liters of water per day, with an average flow of 3 million liters and a recycled discharge of 0.2 million liters, was operated using an 18.1-hour hydraulic retention time. The facility met the most recent effluent standards criteria and was effective in eliminating COD, BOD, NH_4-N, and TSS. The plant has performed well since it was put into service and has consistently produced low values for operating parameters in the effluent. COD, BOD_5, NH_4-N, PO_4-P and TSS removal was 95.2±2.2%, 95.8±2.9%, 97.3±2.1 ,45.5±10.8 and 95.1±1.8%, respectively, in the 3-MLD SBR plant.

Table 4.6: Performance evaluation of the SBR plant from 30th June 2022 to 18th July 2022.

S. No	Parameters	Units	Influent	Effluent
1	pH	-	7.4 ± 0.2	7.5 ± 0.3
2	Color	-	Grey	Color less
3	Odor	-	Foul	Odorless
4	COD	mg/L	355 ± 63	16.2 ± 8
5	BOD	mg/L	165 ± 47	5 ± 3
6	NH_4-N	mg/L	26 ± 3.8	0.7 ± 0.5
7	NO_3-N	mg/L	0.9 ± 0.4	5.8 ± 1.4
8	PO_4-P	mg/L	3.2 ± 0.5	1.7 ± 0.3
9	TSS	mg/L	233 ± 80	9.7 ± 2.4

Figure 4.5: Performance Assessment of 3MLD SBR in terms of COD, NH_4-N, NO_3-N and PO_4-P removal

4.3 Effect of flowrate on COD, NH_4-N, and PO_4-P removal breakthrough curve

Three different flow rates were used to study the dynamic adsorption of COD, NH_4-N, and PO_4-P in all 04 continuous fixed bed columns. Figures 4.6, 4.7, and 4.8 show the breakthrough curves for COD, NH_4-N, and PO_4-P inlet concentrations at 2.5, 5, and 7.5 mL/min flow rates, respectively, at 3.5 cm of bed depth in each of the 04 continuous fixed bed columns. The results demonstrate that the breakthrough time and exhaustion time increased with decreasing flow rate for the elimination of COD, NH_4-N, and PO_4-P. From 2.5 to 7.5 ml min^{-1}, the flow rate rises, the slopes of these graphs reflect a reduction in the time from breakthrough to exhaustion. The COD, NH_4-N, and PO_4-P adsorption breakthrough period in all 04 columns dropped from 17 to 13 h then

further to 11h, 17 to 12, and 17 to 12h then further to 10 hours, respectively correspondingly when the flowrates were increased. The synthesized biochar was successful in treating COD, NH_4-N, and PO_4-P in real wastewater for all of the investigated flow rates. This was supported by the biochar columns' ability to remove these contaminants from the secondary treated waste water. Decreased flowrate may enable prolonged contact time between the designed biochar in the columns and the COD, NH_4-N, and PO_4-P in secondary treated effluent. Therefore, when the flow rate was decreased, COD, NH_4-N, and PO_4-P in the effluents displayed a delayed breakthrough time and lower concentration (40).

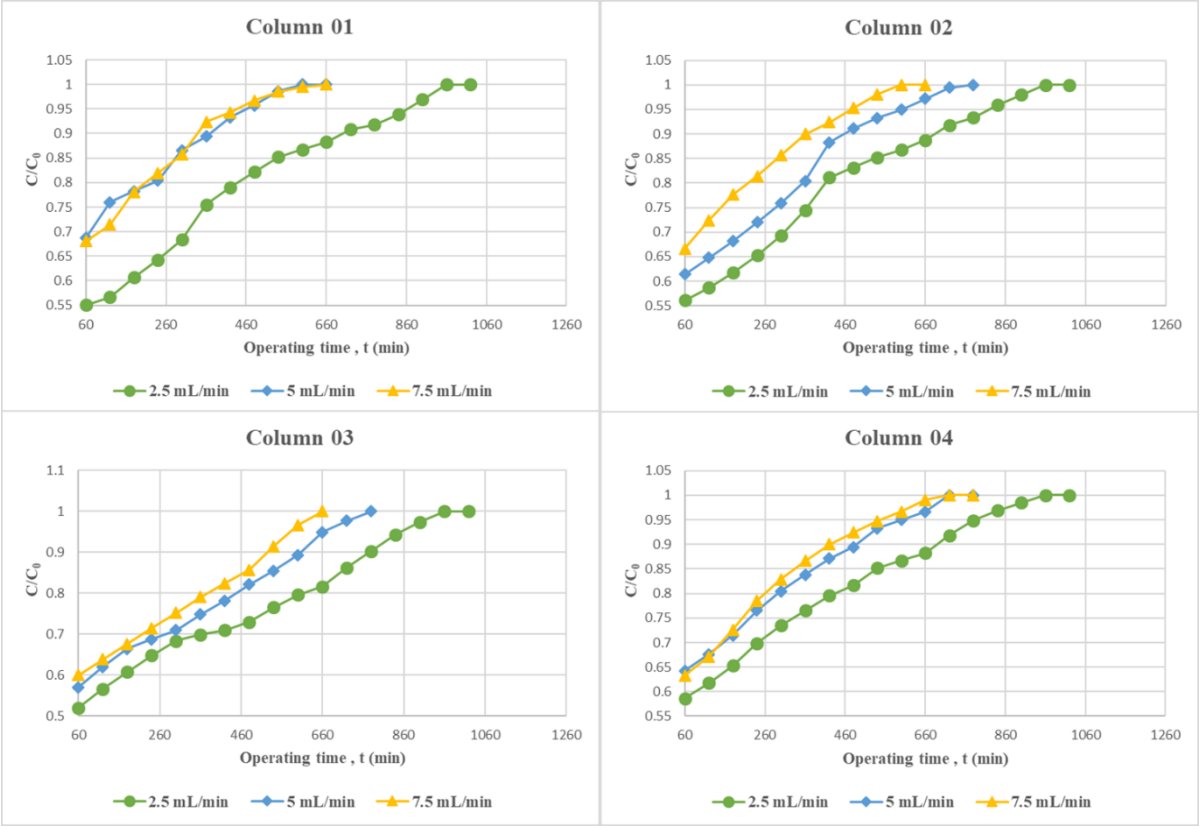

Figure 4.6: Breakthrough curves of COD removal by biochar adsorbent for all 04 columns

This is corroborated by the fact that when the flow rate drops, the breakthrough curves get steeper. Increased contact time of the adsorbate with the biochar leads to greater removal of COD, NH_4-N, and PO_4-P, which may be the cause of the high breakthrough time associated with low flowrates (37).

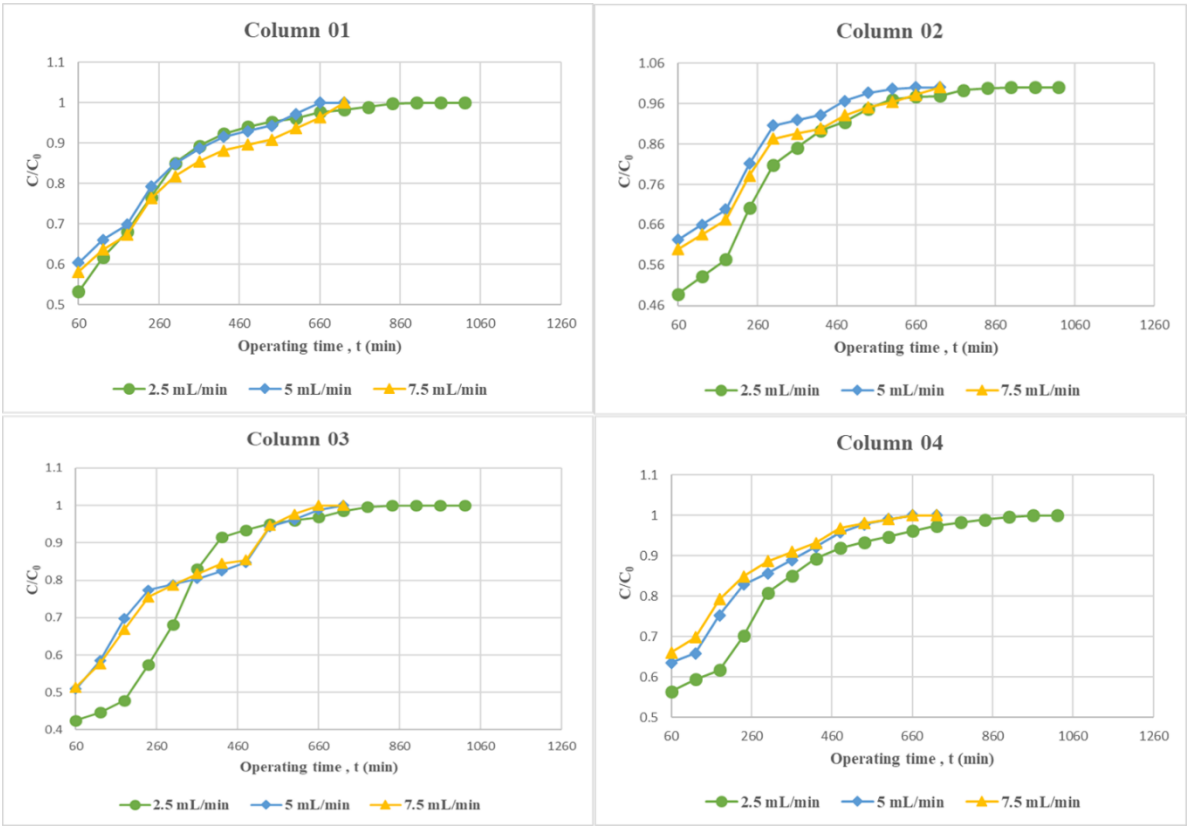

Figure 4.7: Breakthrough curves of NH_4-N removal by biochar adsorbent for all 04 columns

High flow rates cause the mass transfer rate to increase, which accelerates saturation. This is characterised by a decrease in the slope of the curve, which denotes a significant amount of unsaturated zone because of inadequate contact time (37). Adsorbate is removed more quickly from the column when the flowrate is lower because the adsorbate has more opportunity to come into contact with the adsorbent. In general, higher flowrates cause breakthrough points for COD, NH_4-N, and PO_4-P elimination to occur more quickly (38).

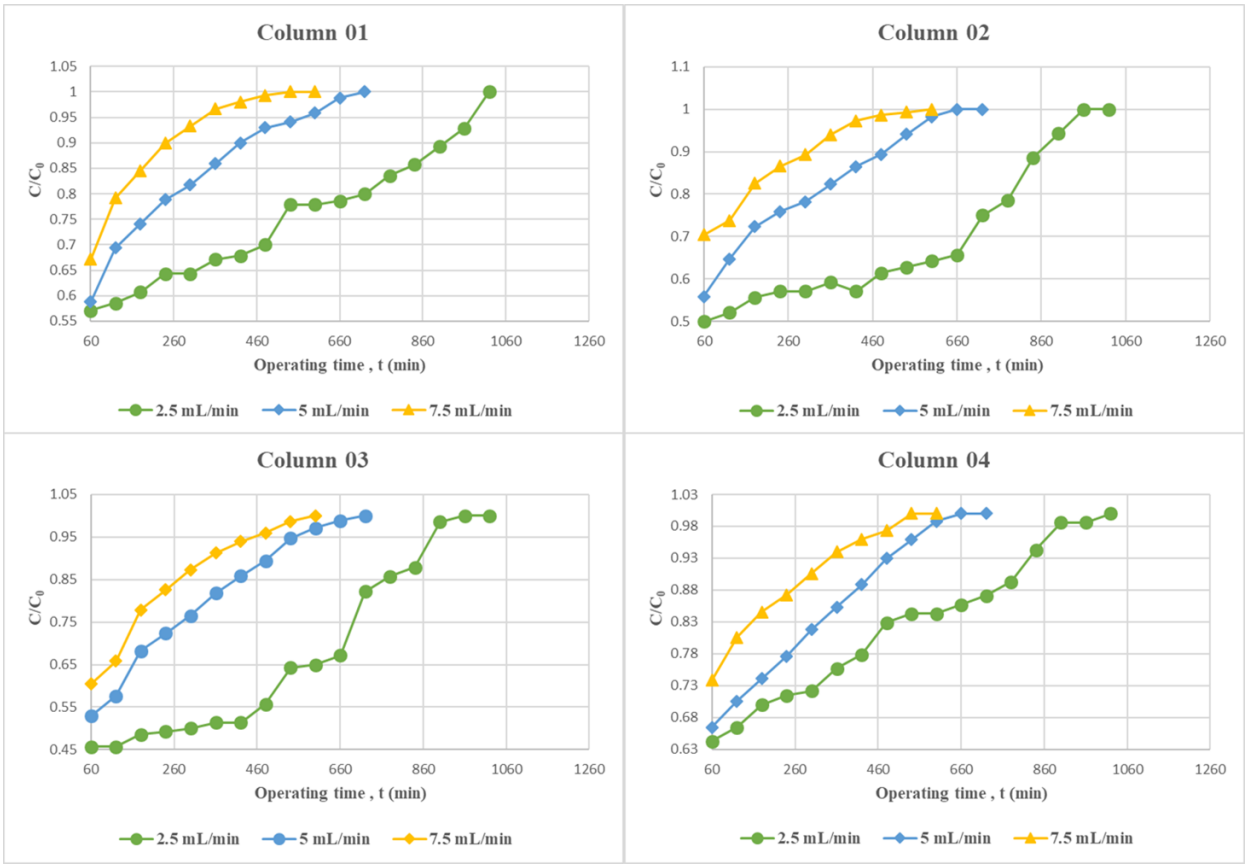

Figure 4.8: Breakthrough curves of PO_4-P removal by biochar adsorbent for all 04 columns

4.4 Effect of initial adsorbate concentration on COD, NH_4-N, and PO_4-P removal breakthrough curve

The effect of initial adsorbate concentration on the breakthrough curve was studied by increasing the initial concentration of COD (19.6, 47.3 mg/L), NH_4-N (0.47, 7, 14.8 mg/L), and PO_4-P (1.4, 3.4, 5.2 mg/L) at flowrate 2.5mL/min as shown in Figure 4.9, 4.10, and 4.11 below. In general, higher initial adsorbate concentrations cause the medium's adsorption sites to saturate more quickly. The breakthrough point occurs earlier as a result, and the concentration of the effluent rises more quickly. Greater mass transfer rates can result from steeper concentration gradients caused by higher initial concentrations. As a consequence, the adsorption kinetics may be accelerated, which might reduce the breakthrough time and speed up the increase in effluent concentration. The initial adsorbate concentration affects how effective the adsorption process is.

Adsorbent removal efficiency may be higher at lower concentrations, leading to a longer breakthrough curve and lower effluent concentrations (43).

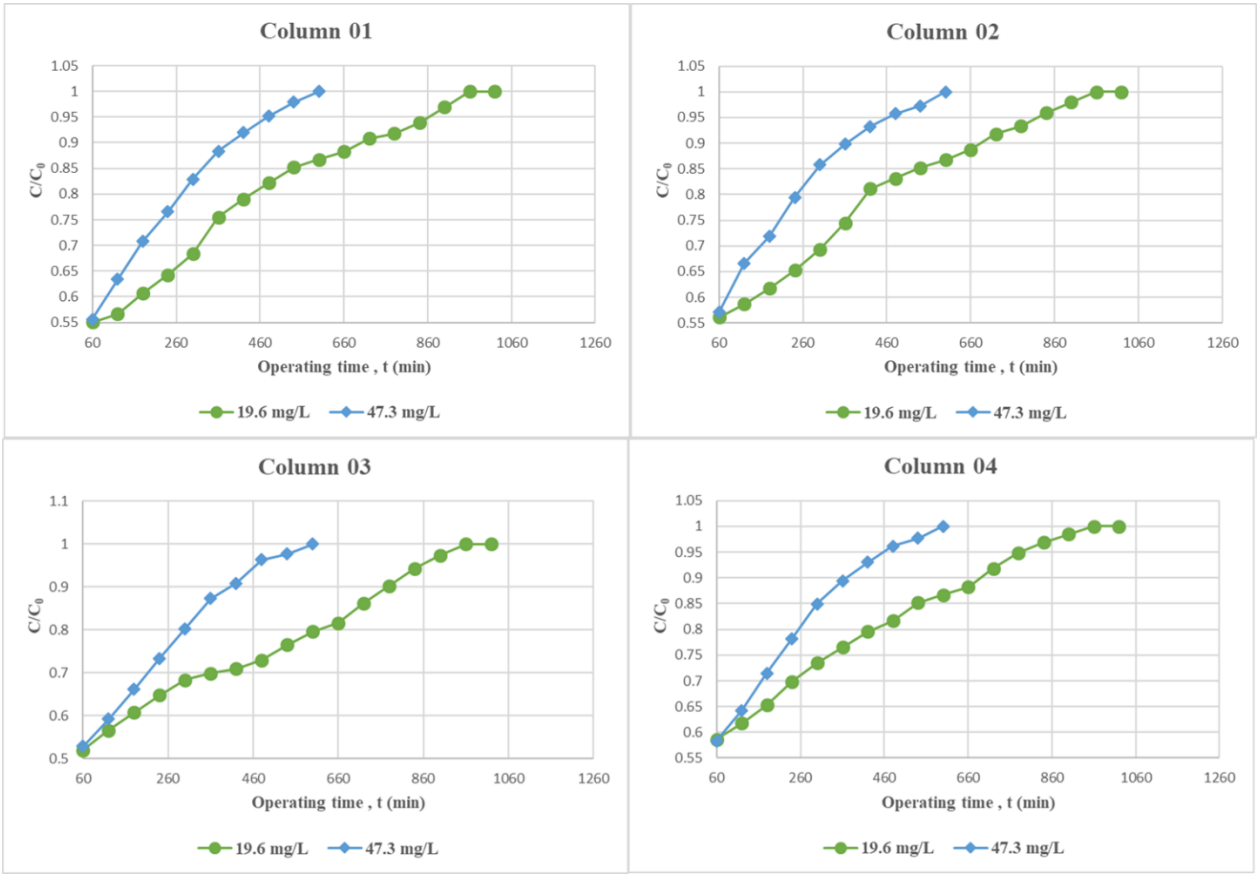

Figure 4.9: Effect of increase in initial concentration on the removal of COD by biochar adsorbent for all 04 columns

The adsorption saturation of biochar was more readily accomplished at higher initial COD, NH_4-N, and PO_4-P concentrations because the adsorption sites on the surface of the biochar were constrained (41). Because more active sites become accessible for the adsorbate as the initial concentration decreases, the increasing trend in adsorption uptake with a drop in initial concentration may be explained (42). The breakthrough curve shown in Figure 5.9 at an initial concentration of 19.6 mg/L shows a more prolonged breakthrough time compared to the curve at 47.3 mg/L of COD. The higher initial concentration is expected to lead to a faster saturation and an earlier breakthrough, resulting in a steeper increase in effluent concentration. The COD adsorption breakthrough period in all 04 columns dropped from 17 to 10 h, correspondingly when the initial COD concentrations increased.

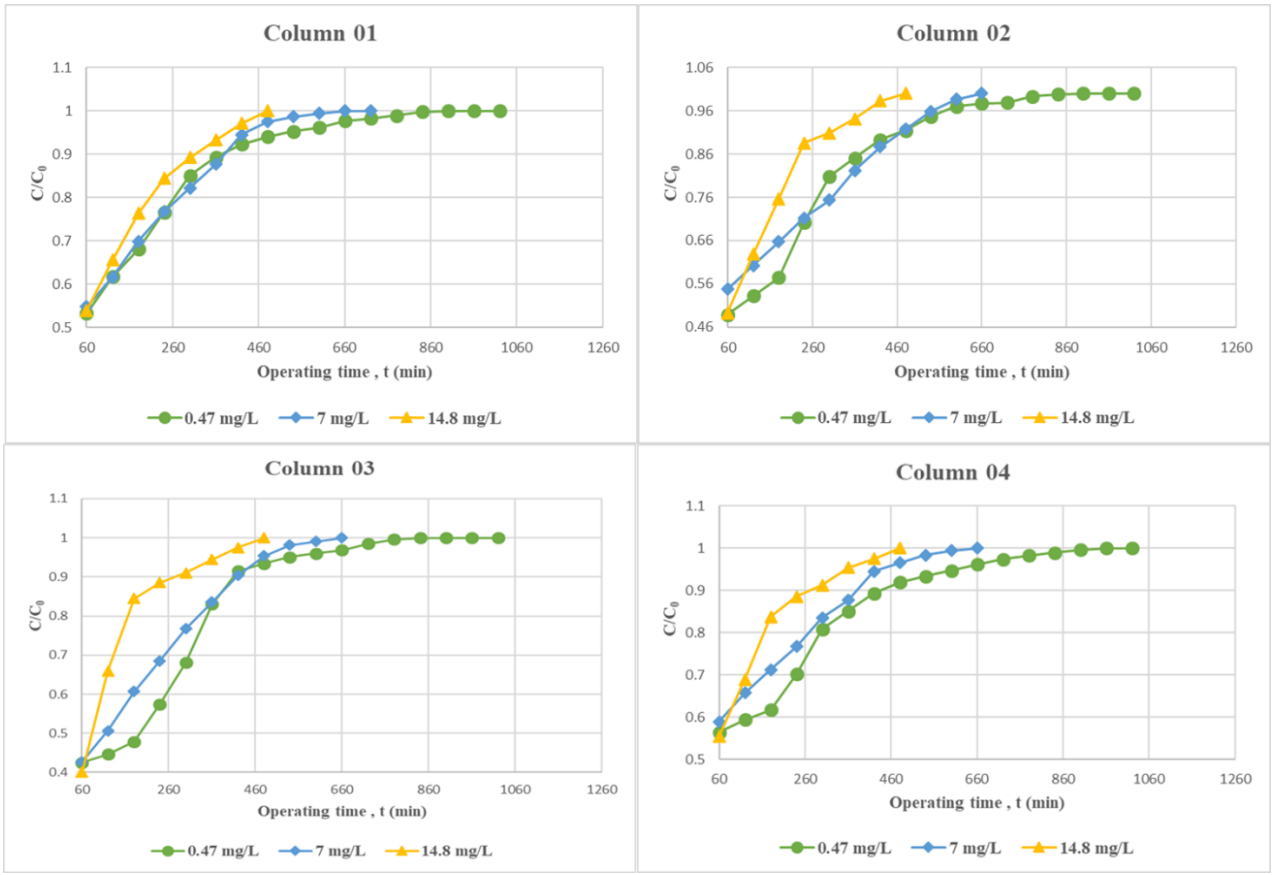

Figure 4.10: Effect of increase in initial concentration on the removal of NH_4-N by biochar adsorbent for all 04 columns

The breakthrough curves as shown in Figure 5.11 at initial concentrations of 1.4 mg/L, 3.4 mg/L, and 5.2 mg/L of PO_4-P would likely exhibit shorter breakthrough times and higher effluent concentrations as the initial concentration increases. The higher initial concentrations would result in a more rapid saturation and earlier breakthrough. This might be explained by the increased influent concentration giving more driving power for the transfer process to get beyond the mass transfer barrier. The PO_4-P adsorption breakthrough periods in all 04 columns dropped from 17 to 12 h then further to 8 h, correspondingly when the initial PO_4-P concentrations increased.

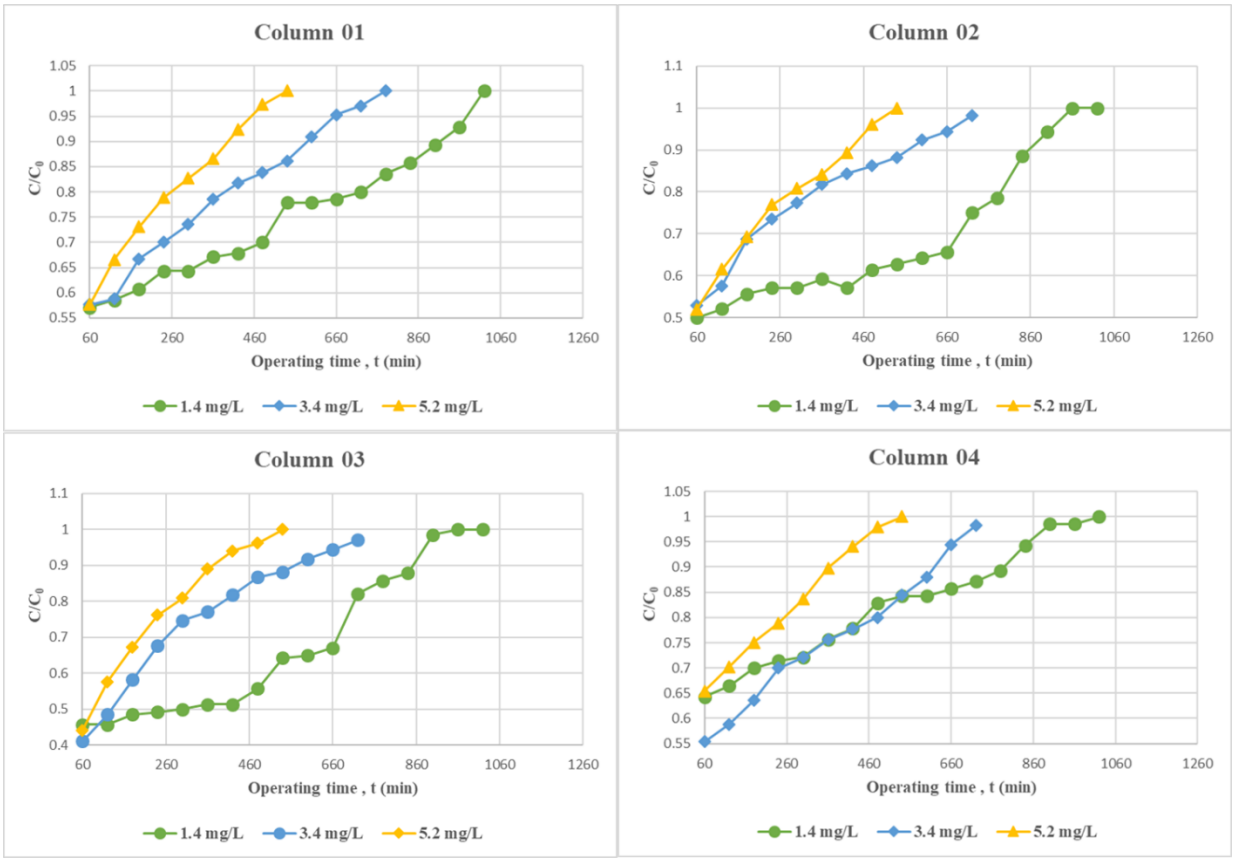

Figure 4.11: Effect of increase in initial concentration on the removal of PO_4-P by biochar adsorbent for all 04 columns

Similarly, the breakthrough curves as shown in Figure 5.10 at initial concentrations of 0.47 mg/L, 7 mg/L, and 14.8 mg/L of NH_4-N show progressively shorter breakthrough times and higher effluent concentrations as the initial concentration increases. Again, the higher initial concentrations would lead to faster saturation and earlier breakthroughs. The NH_4-N adsorption breakthrough periods in all 04 columns dropped from 17 to 13 h then further to 9 h, correspondingly when the initial NH_4-N concentrations increased.

4.5 Dynamic models

Predicting the breakthrough curve for the effluent is necessary for the effective design of a column adsorption process. For the goal of industrial applications, a number of straightforward mathematical models have been created throughout time to describe and analyse lab-scale column

Investigations (44). To determine the optimum model for forecasting the dynamic behaviour of the column, Thomas, Adams-Bohart, and Yoon-Nelson models were developed in this study. These models are useful for understanding and predicting the dynamic behavior of adsorption systems, optimizing process parameters, and designing efficient adsorption processes.

4.5.1 The Thomas model

Under constant bed-depth, variable influent concentration, and variable flowrates, the model was applied to the experimental data. Following Eq. (1), the linear regression analysis was used to determine the relative constants and coefficients, and the results are shown in the table below. R^2 refers to the coefficient of determination. It is a statistical measure that represents the goodness of fit of a regression model. The coefficient of determination is helpful because it indicates the percentage of a variable's variation that can be predicted from the other variables. It is a measurement that enables us to decide how confidently one may draw conclusions from a certain model. The best isotherm model is one in which the coefficient value is closer to unity (45). The higher R^2 values indicate a better fit and a higher level of confidence in the model's ability to explain the adsorption process. In this case, R^2 values are reported for four different columns (01, 02, 03, and 04). R^2 ranges from 0.71 to 0.96, 0.76 to 0.96, 0.67 to 0.99, and 0.80 to 0.98 for columns 01, 02, 03, and 04, respectively.

Table 4.7: Thomas model parameters at different conditions for Column 01

Parameter	Initial Concentration (mg L^{-1})	pH	Flowrate (mL min^{-1})	Bed height (cm)	k_{Th} (mL $min\text{-}mg^{-1}$)	q_o (mg g^{-1})	R^2
COD	19.6	7.8	2.5	3.5	3.5×10^{-5}	84566.3	0.93
	17.9	7.7	5	3.5	2.7×10^{-5}	134821.4	0.86
	21	7.8	7.5	3.5	3.3×10^{-5}	181452.9	0.92
	47.3	7.6	2.5	3.5	2.3×10^{-5}	215683.2	0.92
NH_4-N	0.47	7.8	2.5	3.5	6.3×10^{-4}	2746.5	0.79

	0.53	7.7	5	3.5	1.1×10^{-3}	2011.3	0.94
	0.55	7.8	7.5	3.5	1.09×10^{-3}	2678.5	0.96
	7.3	7.6	2.5	3.5	1.6×10^{-4}	22840.4	0.88
	14.8	7.7	2.5	3.5	1×10^{-4}	31683	0.88
PO_4- P	1.4	7.8	2.5	3.5	3.2×10^{-3}	7730.8	0.71
	1.7	7.7	5	3.5	1.2×10^{-3}	16299.1	0.88
	1.49	7.8	7.5	3.5	1.3×10^{-3}	21193.6	0.79
	3.4	7.6	2.5	3.5	3.8×10^{-4}	20695.7	0.95
	5.2	7.7	2.5	3.5	2.6×10^{-4}	25964.9	0.94

This indicates that the regression model used to describe the adsorption process in column 01 has a good to excellent fit with the experimental data, explaining approximately 71% to 96% of the variance in the data. Similar to column 01, the regression model used for column 02 demonstrates a good to excellent fit with the data, explaining approximately 76% to 96% of the variance. For column 03, the lower end of this range suggests a slightly weaker fit compared to the previous columns, explaining approximately 67% of the variance in the data. However, the higher end of the range indicates an excellent fit with an explanation of approximately 99% of the variance. Column 04, shows a consistently strong fit between the regression model and the experimental data, explaining approximately 80% to 98% of the variance. It was shown that the Thomas model provided a better fitting than the Adams-Bohart model. From the table, it can be seen that k_{TH} for COD, NH_4-N, and PO_4-P initially increased with increasing flow rate at constant bed-depth, but then further decreased. After increasing the initial concentration, k_{TH} decreased at constant flowrate and bed-depth. On the other hand, q_o for COD, and PO_4-P increased with an increase in flowrate at constant bed depth, whereas for NH_4-N initially q_o decreased as the flowrate was increased to 5mL/min at constant bed-depth. q_o saw a corresponding increase for COD, NH_4-N, and PO_4-P at constant bed depth and flowrate of 2.5 mL min^{-1} for increasing initial concentrations

of adsorbate. A maximum bed capacity of 215683.2 mg g^{-1}, 31683 mg g^{-1} and 25964.9 mg g^{-1} were obtained for COD, NH_4-N, and PO_4-P respectively at flowrate of 2.5mL min^{-1} and a bed-depth of 3.5cm with increased initial concentration for column 01. For column 02 maximum bed capacity of 216921.7 mg g^{-1}, 31408.2 mg g^{-1} and 24919 mg g^{-1} were obtained for COD, NH_4-N, and PO_4-P respectively at flowrate of 2.5 mL min^{-1} and a bed-depth of 3.5cm with increased initial concentration.

Table 4.8: Thomas model parameters at different conditions for Column 02

Parameter	Initial Concentration (mg L^{-1})	pH	Flowrate (mL min^{-1})	Bed height (cm)	k_{TH} (mL min-mg^{-1})	q_o (mg g^{-1})	R^2
COD	19.6	7.8	2.5	3.5	3.5×10^{-5}	81849.4	0.93
	17.9	7.7	5	3.5	4.4×10^{-5}	119318.1	0.95
	21	7.8	7.5	3.5	3.3×10^{-5}	185551.9	0.93
	47.3	7.6	2.5	3.5	2.1×10^{-5}	216921.7	0.90
NH_4-N	0.47	7.8	2.5	3.5	8.5×10^{-4}	2311.9	0.82
	0.53	7.7	5	3.5	1.1×10^{-3}	1861.2	0.88
	0.55	7.8	7.5	3.5	1×10^{-3}	2710.7	0.92
	7.3	7.6	2.5	3.5	1.7×10^{-4}	23258.9	0.96
	14.8	7.7	2.5	3.5	1.1×10^{-4}	31408.2	0.83
PO_4- P	1.4	7.8	2.5	3.5	1.4×10^{-3}	4457.2	0.92
	1.7	7.7	5	3.5	1.6×10^{-3}	14515	0.85
	1.49	7.8	7.5	3.5	2×10^{-3}	19567.6	0.76

	3.4	7.6	2.5	3.5	3.8×10^{-4}	14870.7	0.85
	5.2	7.7	2.5	3.5	3.2×10^{-4}	24919	0.92

For column 03 maximum bed capacity of 220357.1mg g^{-1}, 31246.2 mg g^{-1} and 63155.8 mg g^{-1} were obtained for COD, NH_4-N, and PO_4-P respectively at flowrate of 2.5mL min^{-1} and a bed-depth of 3.5cm with increased initial concentration. Similarly for column 04 , maximum bed capacity of 219196.4 mg g^{-1}, 30110 mg g^{-1} and 25749.2 mg g^{-1} were obtained for COD, NH_4-N, and PO_4-P respectively at flowrate of 2.5mL min^{-1} and a bed-depth of 3.5cm with increased initial concentration.

Table 4.9: Thomas model parameters at different conditions for Column 03

Parameter	**Initial Concentration (mg L^{-1})**	**pH**	**Flowrate (mL min^{-1})**	**Bed height (cm)**	**k_{Th} (mL min-mg^{-1})**	**q_o (mg g^{-1})**	**R^2**
COD	19.6	7.8	2.5	3.5	3.5×10^{-5}	91862.2	0.97
	17.9	7.7	5	3.5	4.4×10^{-5}	136120.1	0.99
	21	7.8	7.5	3.5	4.2×10^{-5}	201275.5	0.99
	47.3	7.6	2.5	3.5	2.5×10^{-5}	220357.1	0.94
NH_4-N	0.47	7.8	2.5	3.5	1×10^{-3}	2228.5	0.80
	0.53	7.7	5	3.5	1.1×10^{-3}	2543	0.95
	0.55	7.8	7.5	3.5	1×10^{-3}	4195.9	0.95
	7.3	7.6	2.5	3.5	2.3×10^{-4}	21661.4	0.88
	14.8	7.7	2.5	3.5	1.2×10^{-4}	31246.2	0.67

PO_4- P	1.4	7.8	2.5	3.5	2.5×10^{-3}	8453	0.90
	1.7	7.7	5	3.5	1.5×10^{-3}	15334.5	0.90
	1.49	7.8	7.5	3.5	6×10^{-4}	55084.8	0.88
	3.4	7.6	2.5	3.5	3.5×10^{-4}	9896.6	0.87
	5.2	7.7	2.5	3.5	4.2×10^{-4}	63155.8	0.86

This maximum bed capacity was obtained at the lowest flowrate and a highest initial concentration. The maximum bed capacity occurring at this point can be due to the fact that at lower flowrates, the adsorption capacity is high due to sufficient residence time which allows for effective utilization of the vacant sites before equilibrium is reached (46). Comparing the q_o, it can also be seen that the q_o for COD is higher than NH_4-N, and PO_4-P indicating a higher uptake capacity of the graphene like biochar adsorbent to reduce higher proportions of COD than NH_4-N, and PO_4-P.

Table 4.10: Thomas model parameters at different conditions for Column 04

Parameter	**Initial Concentration (mg L^{-1})**	**pH**	**Flowrate (mL min^{-1})**	**Bed height (cm)**	**k_{Th} (mL $min\text{-}mg^{-1}$)**	**q_o (mg g^{-1})**	**R^2**
COD	19.6	7.8	2.5	3.5	3×10^{-5}	87321.4	0.95
	17.9	7.7	5	3.5	3.9×10^{-5}	121382.7	0.97
	21	7.8	7.5	3.5	3.3×10^{-5}	201785.7	0.91
	47.3	7.6	2.5	3.5	2.1×10^{-5}	219196.4	0.92
NH_4-N	0.47	7.8	2.5	3.5	8.5×10^{-4}	2184.3	0.85
	0.53	7.7	5	3.5	9.4×10^{-4}	1769.5	0.91

	0.55	7.8	7.5	3.5	9×10^{-4}	2772.3	0.91
	7.3	7.6	2.5	3.5	1.5×10^{-4}	22291.6	0.90
	14.8	7.7	2.5	3.5	9.4×10^{-5}	30110	0.80
PO_4- P	1.4	7.8	2.5	3.5	2.6×10^{-3}	7850.7	0.72
	1.7	7.7	5	3.5	1.4×10^{-3}	15019.1	0.90
	1.49	7.8	7.5	3.5	1.6×10^{-3}	19807.1	0.81
	3.4	7.6	2.5	3.5	3.5×10^{-4}	15561.2	0.95
	5.2	7.7	2.5	3.5	2.3×10^{-4}	25749.2	0.98

4.5.2 The Adam-Bohart model

The model was applied to the experimental data under constant bed-depth, variable influent concentration, and variable flowrates. Following Eq. (2), the linear regression analysis was used to determine the relative constants and coefficients, and the results are shown in the table below. In this case, R^2 values are reported for four different columns (01, 02, 03, and 04). R^2 ranges from 0.78 to 0.98, 0.81 to 0.96, 0.70 to 0.99, and 0.80 to 0.98 for columns 01, 02, 03, and 04, respectively. The R^2 range of 0.78 to 0.98 suggests that the regression model for column 01 has a good to excellent fit with the experimental data. This means that the model can explain approximately 78% to 98% of the variance observed in column 01, indicating a high level of effectiveness in capturing the relationship between the independent and dependent variables. The R^2 range of 0.81 to 0.96 indicates that the regression model for column 02 also has a good to excellent fit.

Table 4.11: Adam-Bohart model parameters at different conditions for Column 01

Parameter	Initial Concentration (mg L^{-1})	pH	Flowrate (mL min^{-1})	Bed height (cm)	K_{AB} (mL $min\text{-}mg^{-1}$)	N_o (mg g^{-1})	R^2
COD	19.6	7.8	2.5	3.5	3×10^{-5}	478	0.93
	17.9	7.7	5	3.5	3.7×10^{-5}	610.13	0.86
	21	7.8	7.5	3.5	4.3×10^{-5}	862.9	0.92
	47.3	7.6	2.5	3.5	2.3×10^{-5}	611.1	0.92
NH_4-N	0.47	7.8	2.5	3.5	1.2×10^{-3}	10.1	0.78
	0.53	7.7	5	3.5	1.3×10^{-3}	17.81	0.89
	0.55	7.8	7.5	3.5	1.4×10^{-3}	27.2	0.90
	7.3	7.6	2.5	3.5	1.3×10^{-4}	106	0.89
	14.8	7.7	2.5	3.5	9.4×10^{-5}	156	0.89
PO_4- P	1.4	7.8	2.5	3.5	3.5×10^{-4}	42.8	0.98
	1.7	7.7	5	3.5	4.1×10^{-4}	55.08	0.89
	1.49	7.8	7.5	3.5	4.4×10^{-4}	59.4	0.79
	3.4	7.6	2.5	3.5	3.8×10^{-4}	37.1	0.95
	5.2	7.7	2.5	3.5	2.1×10^{-4}	64.8	0.95

This range implies that the model can explain approximately 81% to 96% of the variance in column 02, signifying a strong relationship between the variables. For column 03, the R^2 range of 0.70 to 0.99 suggests a broader range of fit. The lower end of the range, 0.70, indicates a relatively good

fit, explaining approximately 70% of the variance in the data. However, the higher end of the range, 0.99, suggests an excellent fit, explaining approximately 99% of the variance. This indicates that the model performs well in capturing the relationship between the variables in column 03, with a higher level of explanation at the upper end of the range. Similarly, for column 04, the R^2 range of 0.80 to 0.98 suggests a consistently strong fit. The model can explain approximately 80% to 98% of the variance in column 04, indicating a high level of effectiveness in capturing the relationship between the variables.

Table 4.12: Adam-Bohart model parameters at different conditions for Column 02

Parameter	Initial Concentration (mg L^{-1})	pH	Flowrate (mL min^{-1})	Bed height (cm)	K_{AB} (mL min-mg^{-1})	N_o (mg g^{-1})	R^2
COD	19.6	7.8	2.5	3.5	3×10^{-5}	461	0.93
	17.9	7.7	5	3.5	3.9×10^{-5}	636.9	0.95
	21	7.8	7.5	3.5	4.3×10^{-5}	884.4	0.94
	47.3	7.6	2.5	3.5	2.1×10^{-5}	616	0.90
NH_4-N	0.47	7.8	2.5	3.5	1.9×10^{-3}	8.1	0.81
	0.53	7.7	5	3.5	2.3×10^{-3}	16.7	0.83
	0.55	7.8	7.5	3.5	2.4×10^{-3}	25.9	0.86
	7.3	7.6	2.5	3.5	1.7×10^{-4}	89.8	0.96
	14.8	7.7	2.5	3.5	1.1×10^{-4}	146.1	0.83
PO_4- P	1.4	7.8	2.5	3.5	5×10^{-4}	39.3	0.92
	1.7	7.7	5	3.5	5.7×10^{-4}	55.3	0.92
	1.49	7.8	7.5	3.5	5.9×10^{-4}	55.7	0.90

	3.4	7.6	2.5	3.5	2.3 x10^{-4}	62.8	0.89
	5.2	7.7	2.5	3.5	2.5 x10^{-4}	64	0.94

The experimental data were transformed into the linear form of the Adams-Bohart model by graphing C_f/C_i versus t for COD, NH_4-N, and PO_4-P. The adsorption rate depends on the residual capacity of the adsorbent as well as the concentration of the adsorbate because this model is based on the surface response theory and implies that equilibrium is not immediate. (47). The model's N_o and k_{AB} values have been calculated and are shown in tables for all 04 columns in this section. For all of the examined conditions, COD values are greater than NH_4-N and PO_4-P in comparison. For COD, NH_4-N, and PO_4-P, the values of k_{AB} and No increase as flowrate is increased. (48,49 and 50).

Table 4.13: Adam-Bohart model parameters at different conditions for Column 03

Parameter	**Initial Concentration (mg L^{-1})**	**pH**	**Flowrate (mL min^{-1})**	**Bed height (cm)**	**K_{AB} (mL $min\text{-}mg^{-1}$)**	**N_o (mg g^{-1})**	**R^2**
COD	19.6	7.8	2.5	3.5	3.5 x10^{-5}	447.83	0.98
	17.9	7.7	5	3.5	4.4 x10^{-5}	651.3	0.99
	21	7.8	7.5	3.5	4.8 x10^{-5}	921	0.99
	47.3	7.6	2.5	3.5	2.5 x10^{-5}	638.1	0.94
NH_4-N	0.47	7.8	2.5	3.5	2.7 x10^{-3}	7.8	0.84
	0.53	7.7	5	3.5	3.8 x10^{-3}	16.7	0.88
	0.55	7.8	7.5	3.5	4.7 x10^{-3}	25.2	0.88
	7.3	7.6	2.5	3.5	2.3 x10^{-4}	84.9	0.88

	14.8	7.7	2.5	3.5	1.4 x10^{-4}	134.9	0.70
PO_4- P	1.4	7.8	2.5	3.5	6.4 x10^{-4}	37.07	0.95
	1.7	7.7	5	3.5	7.2 x10^{-4}	57.4	0.92
	1.49	7.8	7.5	3.5	8.6 x10^{-4}	220.6	0.89
	3.4	7.6	2.5	3.5	3.5 x10^{-4}	55.7	0.87
	5.2	7.7	2.5	3.5	3 x10^{-4}	62.1	0.89

The Adam-Bohart model may not be the best model to employ to predict the experimental data under the range of circumstances tested, as seen by the lower values of the $R^2 > 0.70$ observed when compared to the other models investigated. This could be because the Adams-Bohart model is only used in low-concentration areas, and if it were used elsewhere, there would likely be significant differences between the experimental and anticipated curves.

Table 4.14: Adam-Bohart model parameters at different conditions for Column 04

Parameter	**Initial Concentration (mg L^{-1})**	**pH**	**Flowrate (mL min^{-1})**	**Bed height (cm)**	**K_{AB} (mL min-mg^{-1})**	**$N_\circ$ (mg g^{-1})**	**R^2**
COD	19.6	7.8	2.5	3.5	3 x10^{-5}	419	0.95
	17.9	7.7	5	3.5	4.3 x10^{-5}	672.1	0.97
	21	7.8	7.5	3.5	4.8 x10^{-5}	917	0.91
	47.3	7.6	2.5	3.5	2.1 x10^{-5}	628.5	0.92
NH_4-N	0.47	7.8	2.5	3.5	1.4 x10^{-3}	9.1	0.82
	0.53	7.7	5	3.5	2.3 x10^{-3}	15.3	0.89
	0.55	7.8	7.5	3.5	3.2 x10^{-3}	24.1	0.89

	7.3	7.6	2.5	3.5	1.2×10^{-4}	104.5	0.91
	14.8	7.7	2.5	3.5	9.4×10^{-5}	137.7	0.80
PO_4- P	1.4	7.8	2.5	3.5	3.5×10^{-4}	32.2	0.98
	1.7	7.7	5	3.5	4.5×10^{-4}	59.2	0.96
	1.49	7.8	7.5	3.5	5.3×10^{-4}	64.4	0.92
	3.4	7.6	2.5	3.5	2×10^{-4}	69.2	0.96
	5.2	7.7	2.5	3.5	1.7×10^{-4}	67.9	0.98

4.5.3 The Yoon-Nelson model

Under constant bed-depth, variable influent concentration, and variable flowrates, the model was applied to the experimental data. Following Eq. (1), the linear regression analysis was used to determine the relative constants and coefficients, and the results are shown in the table below. In this case, R^2 values are reported for four different columns (01, 02, 03, and 04). R^2 ranges from 0.71 to 0.96, 0.76 to 0.96, 0.67 to 0.99, and 0.80 to 0.98 for columns 01, 02, 03, and 04, respectively.

`

Table 4.15: Yoon-Nelson model parameters at different conditions for Column 01

Parameter	Initial Concentration (mg L^{-1})	pH	Flowrate (mL min^{-1})	Bed height (cm)	K_{YN} (mL min^{-1} mg^{-1}) x 10^{-2}	Ʈ (min)	R^2
COD	19.6	7.8	2.5	3.5	0.36	389.5	0.97
	17.9	7.7	5	3.5	0.64	270	0.91
	21	7.8	7.5	3.5	0.80	254	0.93
	47.3	7.6	2.5	3.5	0.71	260	0.97
NH_4-N	0.47	7.8	2.5	3.5	0.66	285	0.96
	0.53	7.7	5	3.5	0.76	237	0.98
	0.55	7.8	7.5	3.5	0.86	225	0.98
	7.3	7.6	2.5	3.5	0.92	260	0.96
	14.8	7.7	2.5	3.5	0.89	180	0.98
PO_4- P	1.4	7.8	2.5	3.5	0.20	660	0.95
	1.7	7.7	5	3.5	0.58	284	0.94
	1.49	7.8	7.5	3.5	0.96	167	0.97
	3.4	7.6	2.5	3.5	0.45	360	0.93
	5.2	7.7	2.5	3.5	0.69	240	0.92

This indicates that the regression model used to describe the adsorption process in column 01 has a good to excellent fit with the experimental data, explaining approximately 71% to 96% of the variance in the data. Similar to column 01, the regression model used for column 02 demonstrates a good to excellent fit with the data, explaining approximately 76% to 96% of the variance. For column 03, the lower end of this range suggests a slightly weaker fit compared to the previous columns, explaining approximately 67% of the variance in the data. However, the higher end of the range indicates an excellent fit with an explanation of approximately 99% of the variance. Column 04, shows a consistently strong fit between the regression model and the experimental data, explaining approximately 80% to 98% of the variance.

Table 4.16: Yoon-Nelson model parameters at different conditions for Column 02

Parameter	Initial Concentration (mg L^{-1})	pH	Flowrate (mL min^{-1})	Bed height (cm)	K_{YN} (mL min^{-1} mg^{-1}) x 10^{-2}	Ʈ (min)	R^2
COD	19.6	7.8	2.5	3.5	0.39	411.5	0.95
	17.9	7.7	5	3.5	0.62	360	0.89
	21	7.8	7.5	3.5	0.63	275	0.95
	47.3	7.6	2.5	3.5	0.68	230	0.99
NH_4-N	0.47	7.8	2.5	3.5	0.73	270.5	0.96
	0.53	7.7	5	3.5	0.88	240	0.93
	0.55	7.8	7.5	3.5	0.98	223	0.97
	7.3	7.6	2.5	3.5	0.69	246	0.92
	14.8	7.7	2.5	3.5	1.06	170	0.97

PO_4- P	1.4	7.8	2.5	3.5	0.33	720	0.67
	1.7	7.7	5	3.5	0.58	297	0.90
	1.49	7.8	7.5	3.5	0.87	230	0.96
	3.4	7.6	2.5	3.5	0.49	307	0.93
	5.2	7.7	2.5	3.5	0.66	190	0.94

It was demonstrated that the Thomas model fit the data more accurately than the Adams-Bohart model. The k_{YN} and τ values were calculated using the linear version of the Yoon-Nelson model, which is shown in tables for all 04 columns in this section. In general, it can be shown that the KYN for COD, NH_4-N, and PO_4-P increases as the flowrate increases at constant bed-depth. more mass transfer coefficient suggests a more constrained mass transfer zone, more transfer between phases, and hence reduced mass transfer resistance. This suggests that higher values of k_{YN} make COD, NH_4-N, and PO_4-P adsorption simpler. As flowrate is raised, there is a commensurate reduction in the time needed to attain 50% breakthrough. The changes observed can be attributed to reduced residence time associated with high flowrates.

Table 4.17: Yoon-Nelson model parameters at different conditions for Column 03

Parameter	**Initial Concentration (mg L^{-1})**	**pH**	**Flowrate (mL min^{-1})**	**Bed height (cm)**	**K_{YN} (mL min^{-1} mg^{-1}) x 10^{-2}**	**τ (min)**	**R^2**
COD	19.6	7.8	2.5	3.5	0.34	540	0.87
	17.9	7.7	5	3.5	0.45	420	0.87
	21	7.8	7.5	3.5	0.47	380	0.88

	47.3	7.6	2.5	3.5	0.76	270	0.96
NH_4-N	0.47	7.8	2.5	3.5	0.78	330	0.96
	0.53	7.7	5	3.5	0.82	220	0.88
	0.55	7.8	7.5	3.5	0.87	197	0.88
	7.3	7.6	2.5	3.5	0.97	265	0.88
	14.8	7.7	2.5	3.5	1.02	167	0.95
PO_4- P	1.4	7.8	2.5	3.5	0.38	682.7	0.70
	1.7	7.7	5	3.5	0.66	300	0.94
	1.49	7.8	7.5	3.5	0.75	229	0.96
	3.4	7.6	2.5	3.5	0.54	213	0.98
	5.2	7.7	2.5	3.5	0.81	200	0.99

Table 4.18: Yoon-Nelson model parameters at different conditions for Column 04

Parameter	Initial Concentration (mg L^{-1})	pH	Flowrate (mL min^{-1})	Bed height (cm)	K_{YN} (mL min^{-1} mg^{-1}) x 10^{-2}	τ (min)	R^2
COD	19.6	7.8	2.5	3.5	0.40	420	0.92
	17.9	7.7	5	3.5	0.46	350	0.98

	21	7.8	7.5	3.5	0.66	290	0.93
	47.3	7.6	2.5	3.5	0.71	267	0.98
NH_4-N	0.47	7.8	2.5	3.5	0.59	283	0.98
	0.53	7.7	5	3.5	0.72	233	0.97
	0.55	7.8	7.5	3.5	0.82	215	0.97
	7.3	7.6	2.5	3.5	0.86	234	0.94
	14.8	7.7	2.5	3.5	0.92	165	0.98
PO_4- P	1.4	7.8	2.5	3.5	0.35	480	0.81
	1.7	7.7	5	3.5	0.61	336	0.88
	1.49	7.8	7.5	3.5	0.67	230	0.98
	3.4	7.6	2.5	3.5	0.44	390	0.80
	5.2	7.7	2.5	3.5	0.70	290	0.91

CHAPTER 05

CONCLUSION

A number of pollutants can be eliminated from wastewater using the purification method known as adsorption. Adsorption is frequently employed as a tertiary cleaning method following biological water purification to remove non-degradable organic contaminants from groundwater, drinking water preparation, process water, and other drinkable water.

Even though graphene is made from the inexpensive and widely accessible material, graphite, manufacturing is costly and limited. By using biomass waste, this issue may be resolved while the resulting pollution is minimised. One step towards improving graphene technology may be seen in the production of the material employing a green synthesis method. This graphene may then be utilised as a graphene-based adsorbent, and its employment in the field of water filtration involves developing water filters and examining how well they can purify contaminated water for both domestic and commercial uses. The graphene like biochar a adsorbent was successfully synthesized via single-step from agricultural waste i.e., sugarcane bagasse by pyrolysis process in presence of nitrogen gas at 550℃ for 30 min, 45 min, 1 hr., and 1 hr. 15 min. The material was further characterized by Raman spectroscopy, Fourier transform infrared spectroscopy (FTIR), Scanning electron microscopy (SEM) coupled with Energy dispersive X-ray analysis (EDX), and X-ray powder diffraction (XRD). Four experimental columns made of borosilicate glass with an internal diameter of 30 mm and a length of 250 mm. All 04 columns were packed with the different adsorbent materials (35 mm) varying in preparation time viz. 30 min., 45 min., 1 hr., and 1 hr. 15 min. respectively between the supporting layers of glass wool (10 mm) each (for improving the flow distribution and prevention of the loss of adsorbent), and gravel (105mm and 90 mm). The Peristaltic pump RH-P100L-100-4R was used to draw water from the inlet water can to the column. The up-flow mode was used to prevent channeling and assure consistent streaming. columns of diameter 3cm and length 25cm were fabricated with four different materials (varying in their preparation time). The effect of initial adsorbate concentration, and the flow rate of adsorbate in the column were studied for the optimization of the adsorption column setup. Initially, there was an increase in the pH of the adsorbate by 3% for almost one week indicating the release of alkali ions from the adsorbent. The experimental data were fitted with different models such as the

Thomas, Yoon-Nelson and, Adam-Bohart models. Both Thomas and Yoon-Nelson model were found to show a good agreement with the experimental data as compared to Adam-Bohart model. It was concluded that the synthesized green adsorbent could effectively remove COD, NH_4-N, and PO_4-P according to the allowable limits for stringent discharge standards. The sorption of COD, NH_4-N, and PO_4-P was strongly dependent on flowrate and initial concentration of adsorbate. An increase in initial concentration of adsorbate resulted in increased uptake capacity while an increase in flowrate resulted in a reduced uptake capacity for COD, NH_4-N, and PO_4-P. This study has established the potential of using a free, locally and abundantly available waste material for the preparation of graphene like biochar in reducing COD, NH_4-N, and PO_4-P in wastewater.

REFERENCES

1. Rossle WH, Pretorius WA. A review of characterisation requirements for in-line prefermenters: Paper 2: Process characterisation. Water Sa. 2001 Jul 1;27(3):413-22.
2. Reddy KM, Singh SP. Easy removal of nitrate and phosphate anions from water by low cost chitosan and activated charcoal. International Journal of Chemical Reactor Engineering. 2020 Nov 1;18(10-11).
3. RTI Innovation Advisors. "Technology Opportunities for Improved Nutrient Removal from Human Waste." August 2020.
4. Srivastava, G., Rajpal, A., Khursheed, A., Nadda, A.K., Tyagi, V.K. and Kazmi, A.A., 2022. Influence of variations in wastewater on simultaneous nutrient removal in pre-anoxic selector attached full-scale sequencing batch reactor. *International Journal of Environmental Science and Technology*, pp.1-18.
5. Goel, J., Kadirvelu, K., Rajagopal, C. and Garg, V.K., 2005. Removal of lead (II) by adsorption using treated granular activated carbon: batch and column studies. *Journal of hazardous materials*, *125*(1-3), pp.211-220.
6. Kundu, S. and Gupta, A.K., 2005. Analysis and modeling of fixed bed column operations on As (V) removal by adsorption onto iron oxide-coated cement (IOCC). *Journal of colloid and interface science*, *290*(1), pp.52-60.
7. Suman, S., Panwar, D.S. and Gautam, S., 2017. Surface morphology properties of biochars obtained from different biomass waste. *Energy Sources, Part A: Recovery, Utilization, and Environmental Effects*, *39*(10), pp.1007-1012.
8. Biagini, E., Narducci, P. and Tognotti, L., 2008. Size and structural characterization of lignin-cellulosic fuels after the rapid devolatilization. *Fuel*, *87*(2), pp.177-186.
9. Le, P.T., Bui, H.T., Le, D.N., Nguyen, T.H., Pham, L.A., Nguyen, H.N., Nguyen, Q.S., Nguyen, T.P., Bich, N.T., Duong, T.T. and Herrmann, M., 2021. Preparation and Characterization of Biochar Derived from Agricultural By-Products for Dye Removal. *Adsorption Science & Technology*, *2021*.
10. Tohamy, H.A.S., Anis, B., Youssef, M.A., Abdallah, A.E., El-Sakhawy, M. and Kamel, S., 2020. Preparation of eco-friendly graphene oxide from agricultural wastes for water treatment. *Desalin Water Treat*, *191*, pp.250-262.

11. Romero, A., Lavin-Lopez, M.P., Sanchez-Silva, L., Valverde, J.L. and Paton-Carrero, A., 2018. Comparative study of different scalable routes to synthesize graphene oxide and reduced graphene oxide. *Materials Chemistry and Physics*, *203*, pp.284-292.
12. T. Somanathan, K. Prasad, K. Ostrikov, A. Saravanan, V.M. Krishna, Graphene oxide synthesis from agro waste, Nanomaterials, 5 (2015) 826–834.
13. H. Nassef, M. Hagar, Z. Malek, A. Othman, Uptake of tyrosine amino acid on nano-graphene oxide, Materials, 11 (2018) 68.
14. P. Sharma, R. Kaur, C. Baskar, and W.-J. Chung, "Removal of methylene blue from aqueous waste using rice husk and rice husk ash," Desalination, vol. 259, no. 1-3, pp. 249–257, 2010.
15. K. Zhang, P. Sun, M. C. A. S. Faye, and Y. Zhang, "Characterization of biochar derived from rice husks and its potential in chlorobenzene degradation," Carbon, vol. 130, pp. 730–740, 2018.
16. M. Zhang, B. Gao, Y. Yao, Y. Xue, and M. Inyang, "Synthesis, characterization, and environmental implications of graphene-coated biochar," Science of the Total Environment, vol. 435-436, pp. 567–572, 2012.
17. Ghayebzadeh M, Sharafi K, Azizi E, Rahmatabadi S, Pirsaheb M. Removal of nitrogen and phosphorus from municipal wastewater using intermittent cycle moving bed biofilm reactor (ICMBBR). J Chem Pharm Res. 2015;7(6):979-87.
18. Kabuba J, Lephallo J, Rutto H. Comparison of various technologies used to eliminate nitrogen from wastewater: A review. Journal of Water Process Engineering. 2022 Aug 1;48:102885.
19. Mishra S, Singh V, Cheng L, Hussain A, Ormeci B. Nitrogen removal from wastewater: A comprehensive review of biological nitrogen removal processes, critical operation parameters and bioreactor design. Journal of Environmental Chemical Engineering. 2022 Mar 5:107387.
20. Ali I, Alharbi OM, Tkachev A, Galunin E, Burakov A, Grachev VA. Water treatment by new-generation graphene materials: hope for bright future. Environmental Science and Pollution Research. 2018 Mar;25(8):7315-29.
21. Sengupta S, Nawaz T, Beaudry J. Nitrogen and phosphorus recovery from wastewater. Current Pollution Reports. 2015 Sep;1(3):155-66.

22. Hasan MN, Altaf MM, Khan NA, Khan AH, Khan AA, Ahmed S, Kumar PS, Naushad M, Rajapaksha AU, Iqbal J, Tirth V. Recent technologies for nutrient removal and recovery from wastewaters: A review. Chemosphere. 2021 Aug 1;277:130328.
23. Kabuba J, Lephallo J, Rutto H. Comparison of various technologies used to eliminate nitrogen from wastewater: A review. Journal of Water Process Engineering. 2022 Aug 1;48:102885.
24. Boutilier MS, Lee J, Chambers V, Venkatesh V, Karnik R. Water filtration using plant xylem. PLoS One. 2014 Feb 26;9(2):e89934.
25. Ali I, Alharbi OM, Tkachev A, Galunin E, Burakov A, Grachev VA. Water treatment by new-generation graphene materials: hope for bright future. Environmental Science and Pollution Research. 2018 Mar;25(8):7315-29.
26. Goswami S, Banerjee P, Datta S, Mukhopadhayay A, Das P. Graphene oxide nanoplatelets synthesized with carbonized agro-waste biomass as green precursor and its application for the treatment of dye rich wastewater. Process Safety and Environmental Protection. 2017 Feb 1;106:163-72.
27. Bunce JT, Ndam E, Ofiteru ID, Moore A, Graham DW. A review of phosphorus removal technologies and their applicability to small-scale domestic wastewater treatment systems. Frontiers in Environmental Science. 2018 Feb 22;6:8.
28. Lee YD, Shin EB, Choi YS, Yoon HS, Lee HS, Chung IJ, Na JS. Biological removal of nitrogen and phosphorus from wastewater by a single sludge reactor. Environmental technology. 1997 Oct 1;18(10):975-86.
29. Kulakov A, Makisha N. Removal of nitrogen and phosphorous from domestic wastewater. InMATEC Web of Conferences 2017 (Vol. 112, p. 10019). EDP Sciences.
30. Rolf Eliassen and George Tchobanoglous. Removal of nitrogen and phosphorus from, Environmental Science & Technology. June 1969 .536-541
31. Reddy, K. M., & Singh, S. P. (2020). Easy removal of nitrate and phosphate anions from water by low cost chitosan and activated charcoal. *International Journal of Chemical Reactor Engineering*, *18*(10-11).
32. Sengupta, S., Nawaz, T., & Beaudry, J. (2015). Nitrogen and phosphorus recovery from wastewater. *Current Pollution Reports*, *1*, 155-166.

33. Eliassen, R., & Tchobanoglous, G. (1969). Removal of nitrogen and phosphorus from waste water. *Environmental Science & Technology*, *3*(6), 536-541.
34. Dong, Z., & Zhao, L. (2018). Covalently bonded ionic liquid onto cellulose for fast adsorption and efficient separation of Cr (VI): Batch, column and mechanism investigation. *Carbohydrate polymers*, *189*, 190-197.
35. Calero, M., Hernáinz, F., Blázquez, G., Tenorio, G., & Martín-Lara, M. A. (2009). Study of Cr (III) biosorption in a fixed-bed column. *Journal of Hazardous Materials*, *171*(1-3), 886-893.
36. Ahmed, M. J., & Hameed, B. H. (2018). Removal of emerging pharmaceutical contaminants by adsorption in a fixed-bed column: a review. *Ecotoxicology and Environmental Safety*, *149*, 257-266.
37. López-Cervantes, J., Sánchez-Machado, D. I., Sánchez-Duarte, R. G., & Correa-Murrieta, M. A. (2018). Study of a fixed-bed column in the adsorption of an azo dye from an aqueous medium using a chitosan–glutaraldehyde biosorbent. *Adsorption Science & Technology*, *36*(1-2), 215-232.
38. Sheng, L., Zhang, Y., Tang, F., & Liu, S. (2018). Mesoporous/microporous silica materials: preparation from natural sands and highly efficient fixed-bed adsorption of methylene blue in wastewater. *Microporous and Mesoporous Materials*, *257*, 9-18.
39. Ademiluyi, F. T., Amadi, S. A., & Amakama, N. J. (2009). Adsorption and Treatment of Organic Contaminants using Activated Carbon from Waste Nigerian Bamboo. *Journal of Applied Sciences and Environmental Management*, *13*(3).
40. Zheng, Y., Wang, B., Wester, A. E., Chen, J., He, F., Chen, H., & Gao, B. (2019). Reclaiming phosphorus from secondary treated municipal wastewater with engineered biochar. *Chemical Engineering Journal*, *362*, 460-468.
41. Zhang, X., Liu, X., Zhang, Z., & Chen, Z. (2021). Removal of phosphate from aqueous solution by chitosan coated and lanthanum loaded biochar derived from urban dewatered sewage sludge: adsorption mechanism and application to lab-scale columns. *Water Science and Technology*, *84*(12), 3891-3906.
42. Zeinali, F., Ghoreyshi, A. A., & Najafpour, G. D. (2010). Adsorption of dichloromethane from aqueous phase using granular activated carbon: isotherm and breakthrough curve measurements. *Middle-East Journal of Scientific Research*, *5*(4), 191-198.

43. Aksu, Z., & Gönen, F. (2004). Biosorption of phenol by immobilized activated sludge in a continuous packed bed: prediction of breakthrough curves. *Process biochemistry*, *39*(5), 599-613.
44. Chen, S., Yue, Q., Gao, B., Li, Q., Xu, X., & Fu, K. (2012). Adsorption of hexavalent chromium from aqueous solution by modified corn stalk: a fixed-bed column study. *Bioresource technology*, *113*, 114-120.
45. Patel, H. (2019). Fixed-bed column adsorption study: a comprehensive review. *Applied Water Science*, *9*(3), 45.
46. Tan, I. A. W., Ahmad, A. L., & Hameed, B. H. (2008). Adsorption of basic dye using activated carbon prepared from oil palm shell: batch and fixed bed studies. *Desalination*, *225*(1-3), 13-28.
47. López-Cervantes, J., Sánchez-Machado, D. I., Sánchez-Duarte, R. G., & Correa-Murrieta, M. A. (2018). Study of a fixed-bed column in the adsorption of an azo dye from an aqueous medium using a chitosan–glutaraldehyde biosorbent. *Adsorption Science & Technology*, *36*(1-2), 215-232.
48. Brion-Roby, R., Gagnon, J., Deschênes, J. S., & Chabot, B. (2018). Development and treatment procedure of arsenic-contaminated water using a new and green chitosan sorbent: kinetic, isotherm, thermodynamic and dynamic studies. *Pure and Applied Chemistry*, *90*(1), 63-77.
49. Mondal, P., Mehta, D., Saharan, V. K., & George, S. (2018). Continuous column studies for water defluoridation using synthesized magnesium-incorporated hydroxyapatite pellets: experimental and modeling studies. *Environmental Processes*, *5*, 261-285.
50. Xavier, A. L. P., Adarme, O. F. H., Furtado, L. M., Ferreira, G. M. D., da Silva, L. H. M., Gil, L. F., & Gurgel, L. V. A. (2018). Modeling adsorption of copper (II), cobalt (II) and nickel (II) metal ions from aqueous solution onto a new carboxylated sugarcane bagasse. Part II: Optimization of monocomponent fixed-bed column adsorption. *Journal of colloid and interface science*, *516*, 431-445.
51. Nutrients: Phosphorus, Nitrogen Sources, Impact on Water Quality - A General Overview (2018)